DESIGN OF A CLOSED LOOP SYSTEM FOR GLAUCOMA TREATMENT INCLUDING MEASUREMENT OF INTRAOCULAR PRESSURE AND THERAPEUTIC STIMULATION OF THE EYE

by

Rachael A. Swenson

A Thesis

Submitted to the Faculty of Purdue University

In Partial Fulfillment of the Requirements for the degree of

Master of Science in Biomedical Engineering

Weldon School of Biomedical Engineering

West Lafayette, Indiana

May 2019

THE PURDUE UNIVERSITY GRADUATE SCHOOL
STATEMENT OF COMMITTEE APPROVAL

Dr. Pedro Irazoqui, Chair

Department of Biomedical Engineering

Dr. Chi Hwan Lee

Department of Biomedical Engineering

Dr. Hugh Lee

Department of Biomedical Engineering

Approved by:

Dr. George R. Wodicka

Head of the Graduate Program

For my loving Family.

And All the Time God is Good.

ACKNOWLEDGMENTS

This work has been made possible through the support of many people. I would first like to thank my wonderful lab mates in the Center for Implantable Devices (CID). You are always willing to assist me technically and have made my time in the CID enjoyable and productive. A big thank you goes out to my professor Dr. Pedro Irazoqui. Thank you for encouraging and guiding me in my research during my time in the CID and for providing me the opportunity to complete work that I am proud of.

The glaucoma project could not exist without the tireless work of a number of people. Jay Shah has been instrumental to the development of this project and will continue to do great things with it after I am gone. I would also like to thank Brett Collar, Curtis Slaubaugh, Ethan Biggs, and Gabriel Albors. Additionally, Dr. Gabriel Simon has provided inspiration, clinical ophthalmological knowledge, and surgical expertise to this project. He has also dedicated significant amounts of time to the project, flying in from Spain numerous times to work with the team.

Last but not least, I need to thank my family and friends, especially my parents. You have supported and inspired me long before I started my graduate studies. You have shaped me into the person I am today and will continue to support me in the years to come. A special thanks goes out to Garrett Fulton, Marisa Dowling, and Laura Deemer. You three have kept me sane this year.

TABLE OF CONTENTS

LIST OF TABLES

LIST OF SUPPLEMENTARY TABLES

LIST OF FIGURES

LIST OF SUPLEMENTARY FIGURES

ABBREVIATIONS

Analog Front End (AFE)

Analog to Digital Converter (ADC)

Application Specific Integrated Circuit (ASIC)

Aqueous Humor (AH)

Blood Flow (BF)

Center for Implantable Devices (CID)

Complementary Metal-Oxide Semiconductor (CMOS)

Data Acquisition System (DAQ)

Direct Current (DC)

Electrostatic Discharge (ESD)

Episcleral Venous Pressure (EVP)

Flow Rate through the Uveoscleral Pathways (F_{uveo})

Ground (GND)

Inner Diameter (ID)

Intraocular Lens (IOL)

Instrumentation Amplifier (INA)

Intraocular Pressure (IOP)

Low Pass Filter (LPF)

Ocular In-Flow Rate (F_{in})

Outer Diameter (OD)

Outflow Facility of the Trabecular Meshwork (C_{trab})

Pressure (P)

Printed Circuit Board (PCB)

Resistance to Current (R-I)

Resistance to Voltage (R-V)

Resistor (R)

Voltage (V)

Trabecular Meshwork (TM)

ABSTRACT

Author: Swenson, Rachael, A. MSBME
Institution: Purdue University
Degree Received: May 2019
Title: Design of a closed loop system for glaucoma treatment including measurement of intraocular pressure and therapeutic stimulation of the eye
Committee Chair: Pedro Irazoqui

Glaucoma is the leading cause of irreversible blindness worldwide effecting more than 2.7 million people in the U.S alone. Treatments exist in the form of both pharmaceutical and surgical options, but often do not provide the desired efficacy. For example, the failure rate of a trabeculectomy procedure is 39% within 5 years. Additionally, none of the current glaucoma treatments allow for closed loop monitoring of pressure, therefore requiring more frequent doctor visits. Glaucoma management can be improved through the use of a closed loop application of electroceutical treatment. The goal is to develop an implantable device that will be inserted into the eye to monitor intraocular pressure (IOP) and provide responsive therapeutic stimulation to the eye. I designed a discrete pressure monitoring system that interacts with a bare die piezoresistive pressure sensor. The system is based on a Wheatstone bridge design which translates the input resistances of the pressure sensor into a voltage output. This system has an average accuracy of 0.53 mmHg and draws 295 µW of power. I then combined this pressure system with data processing code and Howland current pump stimulation circuitry. This simulation system can output up to 1.05 mA of current for electroceutical intraocular stimulation to lower IOP. Future work will involve miniaturizing the circuitries in the form of an ASIC and packaging the entire system into an ocular implant. This implant can wirelessly monitor IOP and provide therapeutic stimulation to lower IOP. A reliable, closed loop method of lowering IOP would greatly benefit the ever-growing population affected by glaucoma.

1. INTRODUCTION

1.1 Glaucoma

Glaucoma is the global leading cause of irreversible blindness [1] with primary open-angle glaucoma (henceforth referred to as glaucoma) making up 74% of all reported cases [2]. In 2010 the prevalence of glaucoma in the United States was 2.72 million, a 23% increase from 2000 [3]. This global disease is expected to continue to increase in prevalence, affecting the quality of more lives unless better treatments are developed to stop the onset of irreversible optic nerve damage. Glaucoma causes permanent damage to the optic nerve leading to a permanent loss in vision. One of the major risk factors for glaucoma is elevated intraocular pressure (IOP) [4]. It is believed that high pressures within the eye are damaging the optic nerve [3]. Elevated IOP occurs when there is an imbalance in the flow rate of aqueous humor (AH) in and out of the eye [4].

1.1.1 Eye Anatomy

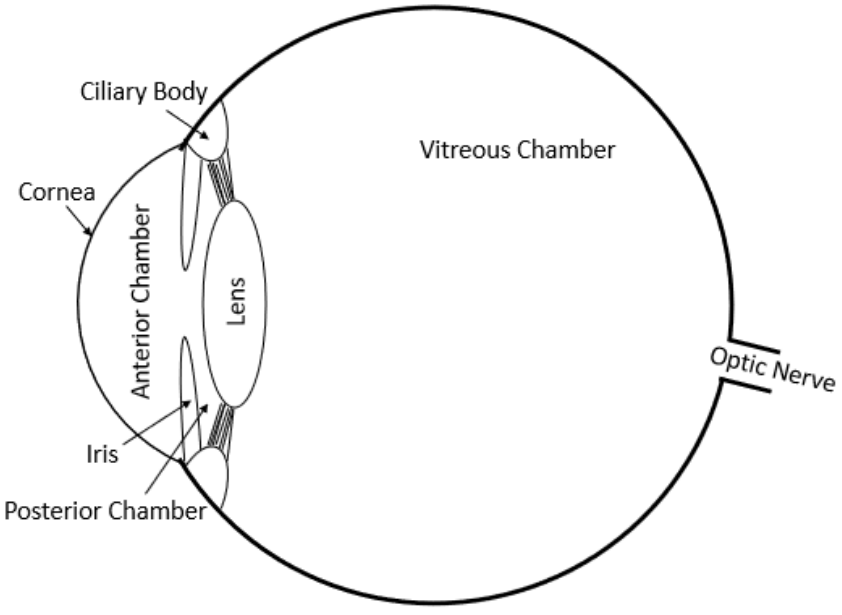

Figure 1: Anatomy of the Eye (not to scale) showing the chambers of the eye and the structures of the eye related to glaucoma and surgical implantation of intraocular lenses.

The eye is divided into three major chambers (see Figure 1). The anterior chamber, located between the cornea and the iris, and the posterior chamber, located between the iris and the lens, are filled with aqueous humor, while the vitreous chamber, located behind the lens is filled with vitreous humor [5]. The intraocular pressure is approximately constant throughout the eye and is controlled primarily through the flow rates of aqueous humor. Aqueous humor is cycled through the eye to deliver nutrients to structures that need to be transparent (such as the cornea) and therefore cannot be reached by blood vessels [6]. The ciliary body produces AH in the posterior chamber and it then flows up through the pupil into the anterior chamber where it leaves through the trabecular meshwork (TM) into Schlemm's canal (see Figure 2). In addition to this pathway, some of the AH will leave and enter the eye through passive transport through the ocular tissues. This passive transport is known as uveoscleral flow. Imbalance of these flow pathways will impact the pressure within the eye [6].

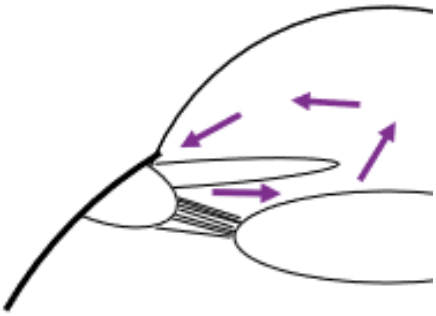

Figure 2: Aqueous Humor Flow within the Eye. The fluid is produced within the ciliary body and exits through the trabecular meshwork after nourishing the structures of the eye.

Studies have shown the outflow of AH is directly related to the contraction of the ciliary body due to antagonism within the ciliary muscle and trabecular meshwork [7]. When the ciliary muscle is contracted, it relaxes the trabecular meshwork and vice versa. This allows the AH outflow rate to be modified by causing contraction of the ciliary muscle.

The pressure within the eye (IOP) can be modeled as a function of the episcleral venous pressure (EVP), the flow rate into the eye (F_{in}), the flow rate out through the uveoscleral (passive transport) pathways (F_{uveo}), and the outflow facility of the trabecular meshwork (C_{trab}) [6]. EVP is dependent on the pressures within the venous system and constant at about 9 mmHg [6].

Therefore, approximately half of a patient's IOP is directly proportional to the resistance ($1/C_{trab}$) to aqueous humor outflow through the trabecular meshwork.

$$IOP = EVP + \frac{(F_{in} - F_{uveo})}{C_{trab}} \quad (1)$$

1.1.2 Effects of Innervation on Aqueous Humor Pathways

The inflow of aqueous humor is controlled by the blood flow to the ciliary body [8]. When ciliary blood flow (BF) is above 74% of its nominal rate, the rate of production of aqueous humor is at its maximum. If BF falls below 74%, the rate of AH production is flow-dependent, decreasing as BF decreases. Aqueous humor outflow is controlled by the resistance within the trabecular meshwork. The resistance within the trabecular meshwork is affected by the constriction of the iris and ciliary body muscles [7].

When the sympathetic nervous system is stimulated through the superior cervical ganglion, vasoconstriction and activation of the dilator pupillae muscle occurs [8]. Vasoconstriction causes a decrease in the production of AH. Conversely, dilation of the pupil causes a slight increase in TM resistance. This decrease in AH outflow is overcome by the decrease in inflow leading to an overall decrease in IOP when the sympathetic nervous system is stimulated.

Stimulation of the parasympathetic nervous system activates both the ciliary ganglion and the pterygopalatine ganglion [8]. The ciliary ganglion constricts the sphincter pupillae muscle and the ciliary body, causing a decrease in TM resistance, increasing the outflow rate. The vasodilation caused by the stimulation of the pterygopalatine ganglion does not change the rate of production of AH assuming the blood flow was originally at normal rates. Therefore, stimulation of the parasympathetic nervous system will also decrease IOP.

1.1.3 Normal and Glaucomatic Intraocular Pressures and Fluctuations

IOP typically follows a 24-hour cyclic pattern, known as diurnal fluctuations [9]. Human intraocular pressure is typically in the range of 10-21 mmHg with diurnal fluctuations in the range of 2-6 mmHg [4]. People with glaucomatic eyes will typically have pressures above 21 mmHg and can have diurnal fluctuations in excess of 10 mmHg [4]. As nominal IOP in the human eye is 15.5 mmHg [10], the average human eye contains 310 uL of aqueous humor [11],

and aqueous humor typically flows at a rate of 2.5 uL/min [6], IOP could change by about 0.125 mmHg/min.

1.1.4 Glaucoma Treatments

Current methods of treatment for glaucoma include eye drops, oral pharmaceuticals, and surgical interventions [12]. Pharmaceutical treatments (both ocular and oral) for glaucoma act to decrease the amount of fluid within the eye. Eye drops are typically prescribed first as they cause less systemic side effects than oral medications, however both treatments will enter the bloodstream and produce systemic effects [12]. Additionally, these medications may not provide fast-acting affects. Ophthalmic timolol, a beta-blocker frequently used for the treatment of glaucoma, typically takes 4 weeks to provide a stabilized effect on IOP [13]. Surgical procedures for glaucoma include trabeculoplasty, where the trabecular meshwork is partially removed to increase AH outflow, cycloablation, where part of the ciliary body is destroyed to reduce the amount of AH inflow, and drainage implant surgeries, where a shunt is placed into the anterior chamber of the eye to drain the aqueous humor [12]. Despite the widespread use of these treatments, there are many limitations to their efficacy. Pharmaceutical treatments do not primarily affect the TM and therefore cannot lower IOP by more than 25% when acting alone [14]. Surgical interventions tend to fail over time with trabeculectomies having a 39% failure rate after 5 years [15]. These statistics show a need for additional, more effective glaucoma treatment methods.

1.2 Intraocular Pressure Monitoring

1.2.1 Piezoresistive Pressure Sensors

Piezoresistive pressure sensors are made using a flexible membrane that changes resistance when introduced to environments with different pressures. This change in resistance allows for pressure changes to be detected when the sensor is placed within an electrical circuit. Piezoresistive sensors are a type of relative pressure sensor, meaning that they detect the changes in the pressure of the environment rather than the absolute pressure. To measure absolute pressure, these sensors must be calibrated by evaluating their outputs at known pressures. These sensors are subject to drift where the baseline output will change over time based on factors unrelated to the pressure of the system, requiring additional periodic calibrations [16] [17]. The

packaging of piezoresistive sensors must also be done carefully; the membrane of the sensor must be exposed to the environment to ensure that it can respond to the pressure changes [18].

1.2.2 Volcano Sensor

The pressure sensor chosen for this device, based on its size and accuracy, is the bared die pressure sensor produced by Phillips Volcano (henceforth referred to as the Volcano sensor) [19]. It is a piezoresistive sensor with a size of 1 mm x 0.25 mm x 0.07 mm (see Figure 3). This sensor can be modeled as two resistive components in series (see Figure 4). The resistances for R_B and R_T are approximately 3.8 and 3.4 kΩ respectively. The resistances of R_B and R_T decrease and increase respectively by ΔR – approximately 1 Ω per 10 mmHg pressure change.

(a) (b)

Figure 3: The bare die pressure sensor created by Phillips Volcano. (a) Photo of the sensor and (b) a drawing of the sensor showing the dimensions of the sensor. The black rectangle on the upper half of the sensor represents the piezoresistive membrane. The three gold rectangles on the bottom half represent the three electrical pads of the sensor (B, CM, and T).

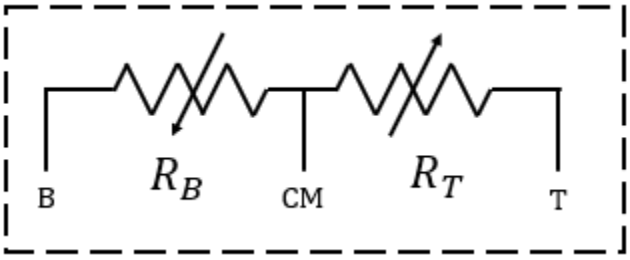

Figure 4: Electrical model of the Volcano sensor consisting of two resistors that vary in opposite directions with respect to pressure. The sensor has three output pads, B, CM, and T.

1.2.3 Implandata Eyemate Device

The most notable device existing on the market for measuring IOP is the Eyemate device, created by the company Implandata. It is an intraocular pressure monitoring system for the management of glaucoma [20]. The Eyemate device records pressure with piezocapacitive sensors enclosed within a silicone ring structure (outer diameter: 11.3 mm, inner diameter: 7 mm, and thickness: 0.9 mm) [21]. The device requires 0.75 mW of power and has a pressure recording error of 0.81 mmHg [21]. This flexible ring is implanted with an IOL during phacoemulsification (see section 1.4) through a 4 mm incision [22]. Eyemate wirelessly transmits the current IOP to an external device, allowing the patient or doctor to monitor the progression of the disease and effectiveness of treatment. This model creates a pseudo-closed-loop environment where the intraocularly monitored pressures can influence the treatment prescribed by a doctor.

1.3 Targeted Electrical Stimulation

An up and coming medical therapy, known as electroceuticals, involves the use of targeted electrical stimulation for the treatment of disease and its symptoms. Muscle and nerve stimulation can be performed using a biphasic current applied across a stimulation and ground electrode pair. Electroceuticals can provide therapy directly to the desired location, thereby increasing the potential effectiveness and decreasing the systematic side effects of the therapy [23].

An electroceutical glaucoma treatment using a specially designed contact lens placed on the surface of the patient's cornea provides an open loop stimulation system to lower IOP [24]. This system, designed by the Center for Implantable Devices (CID), is currently undergoing clinical trials in Barcelona, Spain and Toronto, Canada where promising results have been noted, indicating opportunity for further advancement of this stimulation-based technology for glaucoma treatment [25].

This treatment is also supported by multiple studies in which the stimulation of the ocular nervous system induced decreased IOP. In a study by [26], stimulation of the superior cervical ganglion (sympathetic pathway) was performed with an amplitude of 600 µA (13 Hz, 2.5 ms pulses) showing an immediate pressure drop of nearly 5 mmHg. Additional studies show

stimulation of the sympathetic preganglionic trunk (12 V, 3-12 Hz, 1 ms pulses [27] and 5 V, 20 Hz, 1 ms [28]) to also show significant drops in IOP. The Barcelona trials have used amplitudes between 60-200 µA (50 Hz, 100 µs pulses).

It is believed that these stimulation-based treatments are targeting nervous pathways of the eye to affect the inflow and outflow of aqueous humor. As discussed in section 1.1.2, this can involve either vasoconstriction causing a decrease AH production or stimulation of the ciliary muscle to decrease the resistance of the trabecular meshwork. These scenarios will decrease inflow and increase outflow respectively. By targeting these ocular pathways, electrical stimulation can be used to modulate the pressure within the eye.

1.4 Phacoemulsification Surgical Techniques

The surgery to correct vision impairment due to the presence of cataracts on the crystalline lens of the eye has been developed into a simple microscopic surgery that can be modified for the purposes of implanting an intraocular pressure monitoring and treatment system. In a cataract surgery, or phacoemulsification, the surgeon creates a small incision into the side of the cornea just above the iris [29]. This incision is used to gain access to the interior structures of the eye with a variety of tools. Viscoelastic materials such as methylcellulose are typically used to fill the anterior chamber of the eye and keep the eye inflated [29]. A second incision is made into the capsule surrounding the lens so that a vacuum tool, connected to both a high-pressure saline line and a vacuum line, (see Figure 5) can aspirate the clouded crystalline lens [29] [30]. Using precise surgical technique, the surgeon aspirates lens using the vacuum while the saline replaces any volume lost. Saline is dropped onto the surface of the cornea periodically to keep it hydrated and transparent. Once the lens has been fully removed, an intraocular lens (IOL) is inserted in its place to correct the patient's vision. At the end of this procedure no suturing of other closure methods are needed due to the small size of the incisions [29].

Figure 5: Instrument used for phacoemulsification. The two ports on the proximal end (shown on left) are connected to a vacuum line and a pressured saline line. Both connections run through to the distal tip to evacuate the crystalline lens.

The techniques used by this surgery are optimal for the insertion of an intraocular device into the posterior chamber of the eye. This type of device could likely be placed on top of the crystalline lens without phacoemulsification performed, as a secondary device placed into the posterior chamber during a phacoemulsification procedure, or the device could be integrated into the functional IOL.

1.5 Ideal Closed Loop Intraocular Device for Glaucoma Treatment

There is a need for the development of a closed loop system to provide targeted therapy based on the patient's specific intraocular pressure. Through the combination of microscale piezoresistive sensors and electrical stimulation of intraocular structures, a device can be created to provide treatment to stop the progression of glaucoma in a closed loop format. By integrating wireless powering and data transmission, this device will be fully integrated into the eye and allow for continuous data monitoring (see Figure 6).

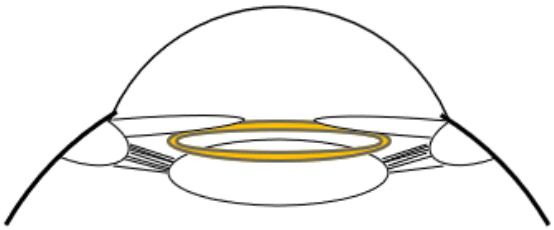

(a)

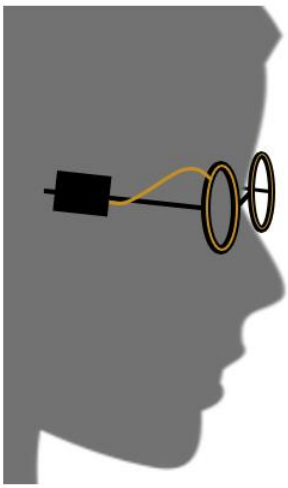

(b)

Figure 6: Mock-up of the ideal device. (a) Intraocular Ring placement inside the posterior chamber of the eye. (b) Stimulation Glasses to provide wireless power transfer to the implanted ring.

In creating this device, the major considerations are pressure sensor accuracy, stimulation circuit capabilities, size of the overall device, wireless powering, and biocompatibility. The specifications defined for these parameters are detailed below and in Table 1.

The pressure sensing accuracy is evaluated based on two specifications, random error and absolute error. The random error is defined by the standard deviations of the pressure data when recorded in a constant pressure environment. Based on the possible rate of change of the eye (1 mmHg in 8 minutes), the standard deviation will be less than 0.5 mmHg over an 8-minute period so that changes will not be buried within the noise floor of the recording. Absolute error, defined by the difference between true and recorded pressure, is less than 1 mmHg. Both metrics correspond to data averaged to no more than a 1-minute sampling period. These specifications

are defined based on the expected possible rate of change of IOP and the physiological pressure defining abnormal IOP as discussed above. Based on the stimulation parameters used in [28] and previous work with electrical stimulation of the eye, the intraocular device will need to be able to provide up to 1 mA of biphasic current.

In evaluating the size of the overall device, it must fit within the posterior chamber and fit through the phacoemulsification incision in the cornea. The specification for the inner diameter of the device is defined by the maximum pupil diameter – 8 mm [31]. This will keep the device from interfering with the patient's vision. To ensure the intraocular ring fits within the desired space, the maximum size of typically implanted IOLs, 14 mm, is used to define the specification of the device [32]. The intraocular ring thickness must be less than the thickness of the adult human crystalline lens in the anteroposterior dimension – 5 mm [33]. The corneal incision size for phacoemulsification is typically under 3 mm, with studies showing that smaller incisions produce the best long-term results [34]. The device most similar to ours, Implandata's Eyemate, has an incision size of 4 mm [22]. Based on this information, the specification for the intraocular ring is to have a maximal incision size of 4 mm, with efforts made to minimize the incision size.

In order to be an implantable device, the intraocular ring must be able to be wirelessly powered. This requires a low power application. It is estimated that at least 5 mW of power will be able to be transferred to the device. In addition, as an implantable device, it must be biocompatible with the interior of the eye. The specification for the biocompatibility is that all materials used should be biocompatible or coated completely in biocompatible materials.

Table 1: Optimal Metrics for the Closed Loop Intraocular Device.

Parameters	**Specification**	
Pressure Sensor Accuracy	Random Error	< 0.5 mmHg
	Absolute Accuracy	< 1 mmHg
Size	Inner Diameter	> 8mm
	Outer Diameter	< 14 mm
	Thickness	< 5mm
	Folded Width	< 4mm
Stimulation	Stimulation Current	> 1 mA
Biocompatibility	Materials	Biocompatible
Wireless Powering	Power Draw	< 5 mW

2. METHODS

2.1 Pressure Sensing Circuitry

To design this device, I first focused on the pressure sensing circuitry. The closed loop intraocular ring will base its therapeutic stimulation patterns on the current pressure measured inside the eye. This requires a highly accurate pressure sensing system. To compare the accuracy of the circuitries the random error metric (see Table 1) was evaluated as the average of the standard deviations of 8-minute time periods recorded under constant pressure environments. This metric is reported as the mean of the random errors ± the standard deviation of the random errors for a given circuit. Each circuit is calibrated by measuring the output of the circuit at multiple environmental pressures within the range of operation (0-60 mmHg). A linear regression model is fit to the data and used to calibrate the output voltage to its corresponding pressure.

In many cases, fixed resistors were used in favor of the Volcano pressure sensor to minimize potential sources of error from changes in absolute pressure. When this was done, I picked resistors to match the expected resistance range of the Volcano Sensor. I used potentiometers to increase and decrease the baseline resistances to mimic pressure changes. Using the conversion factor of 1 Ω per 10 mmHg, the input resistance can be calibrated to a corresponding relative pressure. The fixed resistors effectively imitate the Volcano sensor. A comparison of the two resistance setups, measuring resistance with an LCR meter (Agilent E4980A Precision LCR Meter), shows the unaveraged error of the Volcano sensor is 0.858 ± 0.257 mmHg (n = 478) as compared to a 0.762 ± 0.253 mmHg (n = 103) relative error of fixed resistors.

Other important metrics for pressure sensing circuitry include the size constraints of the posterior chamber of the eye and power consumption for wireless powering. Due to these metrics of size and power consumption, a fully off-the-shelf system would not meet the necessary criteria. Therefore, I designed a discrete sensing system that can be miniaturized into a fully implantable device in the form of a custom ASIC (application specific integrated circuit).

2.1.1 Resistance to Current Circuits

Previous work in the CID lab resulted in the creation of an ASIC (referred to as Hansraj's ASIC) to wirelessly monitor pressure [35]. This circuit converted the resistance of the connected piezoresistive sensor to current, to frequency, and then to a digital transmission signal. To test the ASIC, I wire-bonded (Kulicke and Soffa Model 4526 Wire-Bonder) it to a PCB breakout board. This device was tested by powering a 1.8 V linear regulator (Analog Devices ADP150) with a 5 V source from a DC power supply (Keysight E3631A). The output of the linear regulator powers the ASIC (as shown in Figure S1).

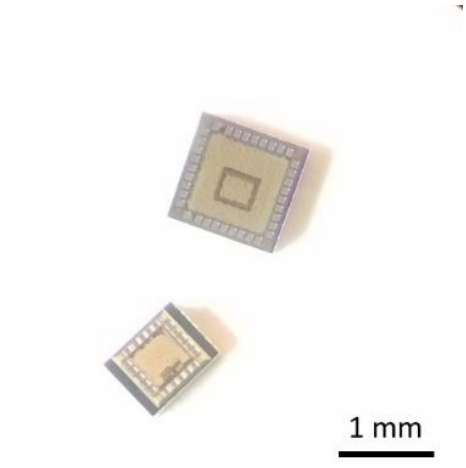

Figure 7: Pressure sensing ASICs created by the CID used in my testing of the circuitry showing Hansraj's ASIC (bottom left) and AFE1 (top right).

The digital transmission output signal of the ASIC is captured using a horn antenna that feeds into a spectrum analyzer (Agilent E4404B). This is used to output the 0 Hz span signal into a comparator circuit and the into a DAQ (National Instruments USB 6353) which is controlled by a script using MATLAB 2018a to decode the digital data into the monitored pressure (see Figure 8).

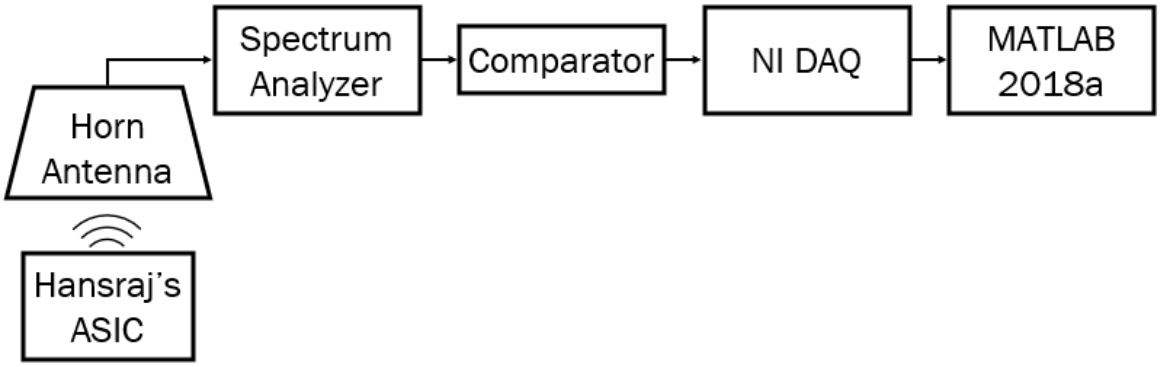

Figure 8: Block Diagram of data processing from output of Hansraj's ASIC.

The digital data is encoded in a 24- or 30-bit packet [23]. The first 4 bits are a header sequence that identifies which type of packet is being sent (R_B, R_S, or R_{diff}). The next bit is the flip bit; when this bit is a '1,' the bits of the data sequence has been flipped. The next sequence is the data; for the R_B or R_S packets the data sequence is 18 bits and represents the frequency (calculated based on the input resistances, the frequency is calculated from the data using equation (2)), while for the R_{diff} packets the data sequence is 12 bits of signed binary and when added to the most recent R_s it represents the frequency. The next 3 bits is the CRC for confirming that the packet has been received correctly. The final 4 bits is the tail sequence which marks the end of the packet.

$$f = \frac{Data}{350} * f_{Bits} \tag{2}$$

The MATLAB code uses the above information to decode the data packets into their respective frequencies. The frequencies are then calibrated to the pressure using linear regression. Testing of this device resulted in measurement errors of nearly 5 mmHg when testing with fixed resistors (see Table 2 for errors of all circuits).

As the error of the fixed resistors and the Volcano sensor are comparable when tested with the same circuitry, and the error is significantly greater using Hansraj's ASIC as compared to the LCR meter (see Figure 9). This suggests that the error in the measurement system is primarily due to the measurement circuit rather than the Volcano sensor itself.

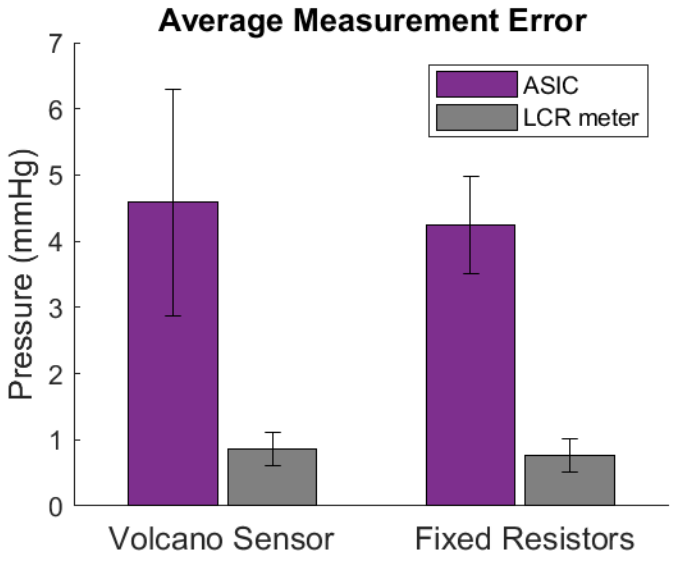

Figure 9: Measurement error of the Volcano sensor and fixed resistors when tested using Hansraj's ASIC and the LCR meter (N = 711, 478, 426, 103 respectively).

To eliminate possible sources of error in this measurement, I tested a different ASIC of only the resistance to current (R-I) analog front end (AFE) block (see Figure 10). This test helps to determine where Hansraj's ASIC, the error primarily comes from. This device was wire bonded to a test PCB (designed in Altium) and powered using 1.8 V and 1.4 V voltages from the benchtop DC power supply (schematic in Figure S2). The output currents of AFE 1 are measured with a picoammeter (Keithley Model 6485 Picoammeter) controlled using a LabVIEW 2016 script. The output currents are linearly related to the environment pressure for calibration. Testing of AFE 1 showed that most of the error of Hansraj ASIC is produced within the R-I block as the error did not show a clinically significant decrease. Similar results were noted with the higher power (2x and 4x power) outputs of the AFE 1 ASIC. Another R-I system (AFE 2 – see Figure S3), previously discarded due to high power consumption, was tested in the same manner as AFE 1. This device produces less measurement error than AFE 1 but is still above the accuracy specification.

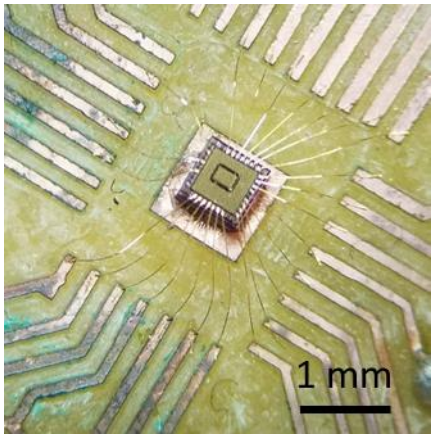

Figure 10: AFE 1 wire-bonded onto a test PCB.

As none of the previously created systems seem likely to meet the desired specification for accuracy, additional analog front ends were created discretely using off the shelf components. The discrete R-I circuits were tested using the same methodology described above for testing the AFE 1 ASIC. As these discrete systems inherently have more noise than the optimized ASICs, the discrete version of AFE 1 was evaluated as a baseline between the ASIC and discrete circuits.

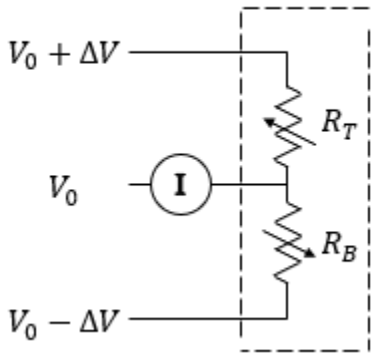

Figure 11: Circuit Schematic of the discrete system for testing the Volcano sensor (shown within the doted box) by turning the resistance into a current. The voltages V0 ± ΔV represent the voltages applied by the power supply. The picoammeter is represented in the figure by the circled 'I.'

The circuit used to monitor the pressure sensor resistance by converting it into a current, as done in the discrete version of AFE 1, is shown in Figure 11. The current is related to the input resistances by equation (3).

$$I_{OUT} = \Delta V \frac{R_B - R_T}{R_B R_T} = \Delta V \frac{R_{B0} - R_{T0} - 2\Delta R}{R_B R_T} \quad (3)$$

Given that R_B and R_T are significantly greater than ΔR, the current is related to ΔR in an approximately linear fashion. Discrete versions of AFE 1 were modified using voltage references to eliminate input noise and by increasing the power consumption (2.5x power) of the circuit.

2.1.2 Resistance to Voltage Circuits

As none of these improvements provided the necessary decrease in error, I designed additional discrete AFEs using a resistance to voltage (R-V) layout as shown in Figure 12. To increase the resolution of the output, the circuit had a 200x gain on the output using an instrumentation amplifier (Texas Instruments INA333). These discrete AFE configurations were powered using the DC voltage supply and the outputs measured using a MATLAB script and the NI DAQ. The output voltages of the R-V circuits are linearly related to the environmental pressure for calibration.

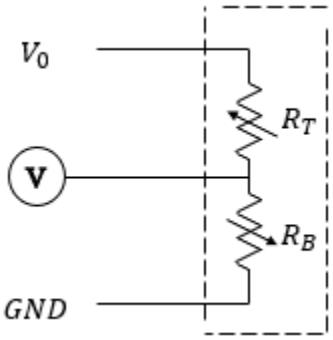

Figure 12: Circuit Schematic of the discrete system for testing the Volcano sensor (shown within the doted box) by turning the resistance into a voltage. The voltages V_0 and GND represent the voltages applied by the power supply. The DAQ is represented in the figure by the circled 'V.'

The output current of the R-V circuits is related to the input resistance based on equation (4). This equation linearly relates the output voltage to the change in resistance and therefore to the change in pressure. In an attempt to further decrease the error of the R-V circuits, I added a 5 Hz Low Pass Filter (LPF) to the output of the circuit.

$$V_{OUT} = V_0 \frac{R_B}{R_B + R_T} \quad (4)$$

2.1.3 Wheatstone Bridge Design

As the discrete and ASIC systems I tested do not providing satisfactory accuracy, reverse engineering techniques were employed. The SurgiVet invasive blood pressure monitor (see Figure 13) distributed by Smiths Medical [36] has been successfully used in the lab to provide accurate pressure measurements (less than 2 mmHg error without averaging at 10 Hz). These devices as well as similar sensors produced by Cobe Laboratories [37] were taken apart to understand their pressure measurement circuitry. Reverse engineering of these devices shows that they use piezoresistive pressure sensors and have the sensors in a Wheatstone bridge configuration with additional stabilization filters (internal circuit boards shown in Figure 14).

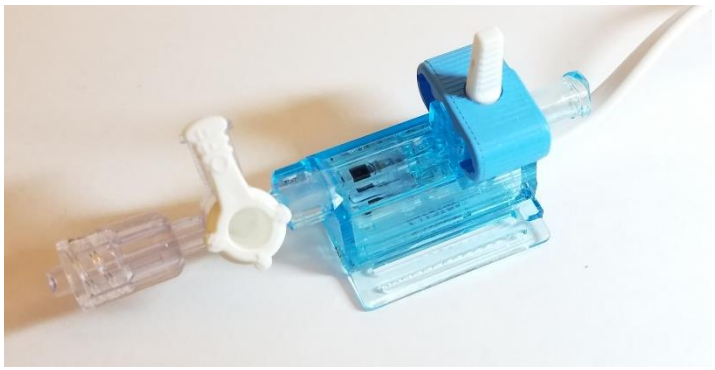

Figure 13: SurgiVet Invasive Pressure Sensor. When monitoring IOP, the lure lock connection on the right end is connected to the cannula and the wire (left side) is connected to the power supply and outputs the recorded voltage.

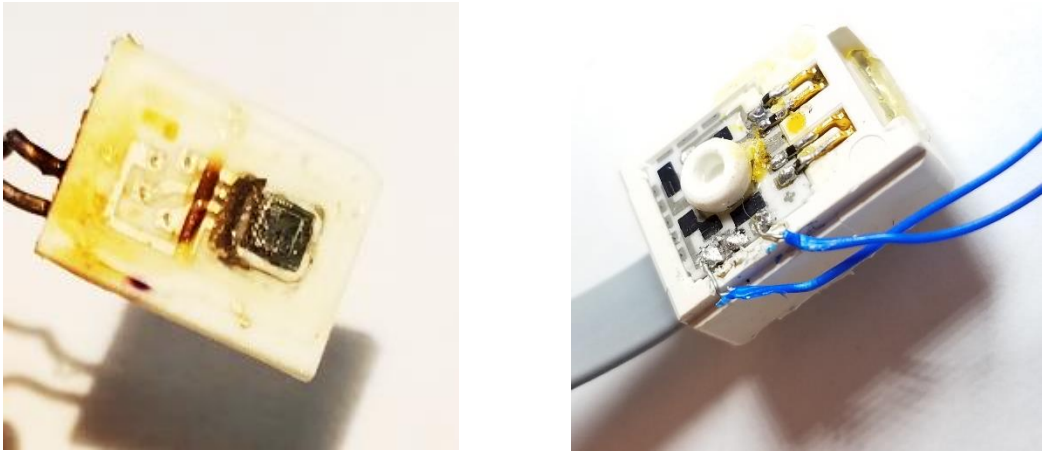

(a) (b)

Figure 14: Internal circuitry of the SurgiVet (a) and Cobe Laboratories (b) pressure sensors. These sensors show the piezoresistive sensor (black square in figure (a)). The silver traces in the figures make up the rest of the Wheatstone bridge circuitry.

I used this design to create a Wheatstone bridge AFE circuit. The discrete version of the Wheatstone bridge discrete circuit is shown in Figure 15. These circuits are powered and monitored using the same techniques as the R-V AFEs. The output voltage is related to the sensor's resistances by equation (5), linearly relating the output voltage to the change in resistance.

$$V_{OUT} = V_1 \frac{\Delta R}{R_T + R_B} Gain \tag{5}$$

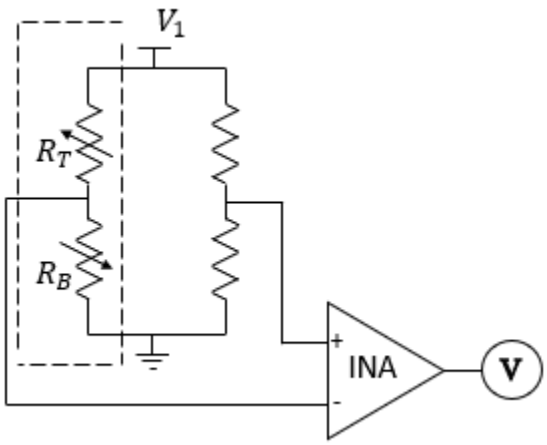

Figure 15: Circuit Schematic of the discrete Wheatstone bridge system for testing the Volcano Sensor (shown within the doted box) by turning the resistance into a voltage. The voltage V_1 represents the voltage applied by the power supply. The DAQ is represented in the figure by the circled 'V.'

To calculate the pressure based on the output voltage of the Wheatstone bridge, equation (6) can be used based on the theoretical parameters. This calibration can also be defined through empirical testing by recording the voltage at known pressures and using regression to create a calibration equation. The empirical calibration was used to evaluate the error of the Wheatstone bridge AFE. The error on this AFE with a 1000x gain using an instrumentation amplifier is under 2 mmHg.

$$PressureCalibation = \frac{(R_B + R_T)10 \text{ mmHg}}{V1 * Gain} \tag{6}$$

Due to the accuracy needed and the potential problems with matching resistors to the Volcano sensors' base resistance, it would be convenient to create the AFE using two Volcano sensors rather than matching resistors to the necessary values. To make the Wheatstone bridge work,

they must be oriented inversely – if not both sides of the Wheatstone bridge will increase and decrease complementary. When testing the volcano sensors in the inverse orientation it was noted that they may have ESD (electrostatic discharge) protections causing them not to behave purely resistive in the reverse orientation.

If the sensor was purely resistive, it would be expected that when a voltage difference, V_{DD}, was placed across the B and T terminals of the pressure sensor the absolute value of the voltages (equations (7) and (8)) across the sensor resistors would be the same regardless of which terminal the high voltage was applied at.

$$V_B = \frac{V_{DD} R_B}{R_B + R_T} \tag{7}$$

$$V_T = \frac{V_{DD} R_T}{R_B + R_T} \tag{8}$$

However, when I tested this in a constant pressure environment, I showed that when the high voltage was placed on the B terminal, the voltages did not respond as expected as VDD was increased (see Figure 16 and Table S1). This test was done by setting a voltage (V_{DD}) on a DC voltage source and connecting the two outside terminals of the Volcano Sensor (B and T) to V_{DD} and GND. I then used a voltmeter to measure the voltage drop across both R_B and R_T. I then flipped the orientation of V_{DD} and GND with respect to the Volcano sensor and measured the voltage drops across R_B and R_T again. These measurements were repeated for multiple V_{DD} voltages.

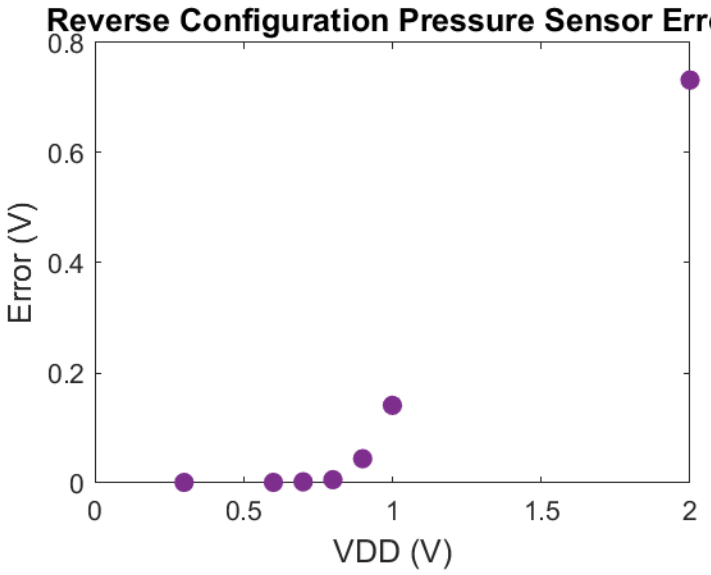

Figure 16: Volcano Sensor Error (Expected Voltage across R_T – Actual Voltage across R_T) when the higher voltage is applied to terminal B.

Based on these results and discussions with engineers at Phillips, it is postulated that ESD protections exist on these sensors and therefore they will not work correctly in the reversed configuration. Thus, the Wheatstone bridge must be designed using resistors that are well matched to R_B and R_T.

During testing, I noted that 60 Hz noise was coupling onto the signal. To clean up the signal I added a 15 Hz LPF before and after the instrumentation amplifier. As the intended signal to be recorded is eye pressure, which does not change quickly (expected to be less than 0.125 mmHg per minute), the low pass frequency can be small to filter out many possible sources of noise.

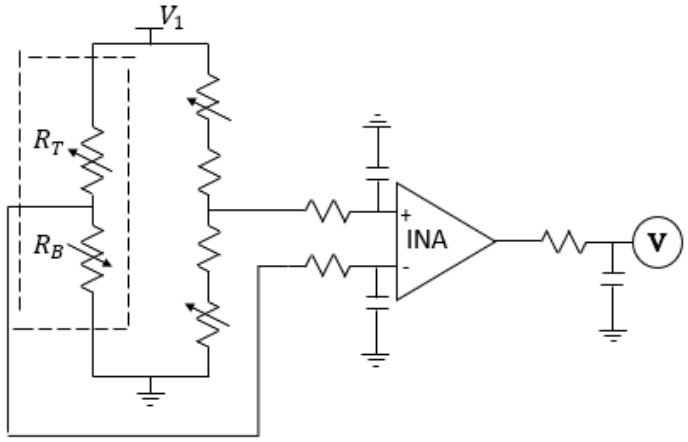

Figure 17: Circuit Schematic of the discrete Wheatstone bridge system with added low pass filters (15 Hz) for testing the Volcano sensor (shown within the doted box) by turning the resistance into a voltage. The voltages V_0 and GND represent the voltages applied by the power supply. The DAQ is represented in the figure by the circled 'V.'

With the low pass filters, the error in the signal is below 0.5 mmHg when V1 is at least 0.2 V-1.8 V and the amplifier has a gain of 1000x (see Figure 18 and Table 3).

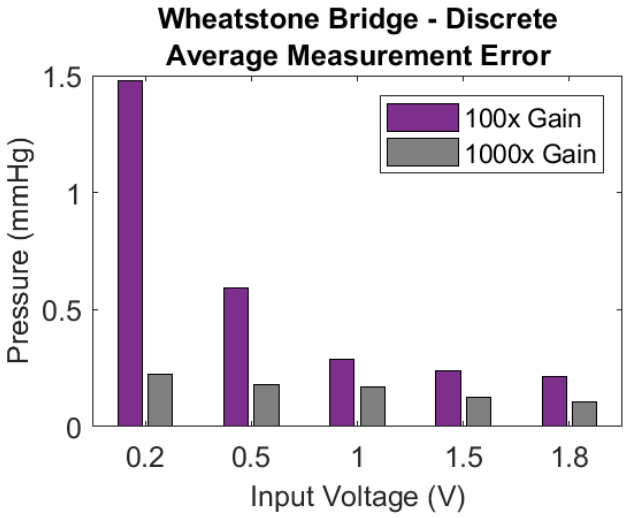

Figure 18: Measurement Error (over 5 minutes, N = 1) of the output of the filtered Wheatstone Bridge circuit given various values of V1 and various amplifier gains.

2.2 Closed Loop Implementation

The final implant device will implement both the pressure sensing and therapeutic stimulation in a closed loop device (see Figure 19). The pressure is to be read from the eye and evaluated to

determine if the pressure is too high. In this case, the stimulation should be applied in the eye to lower pressure.

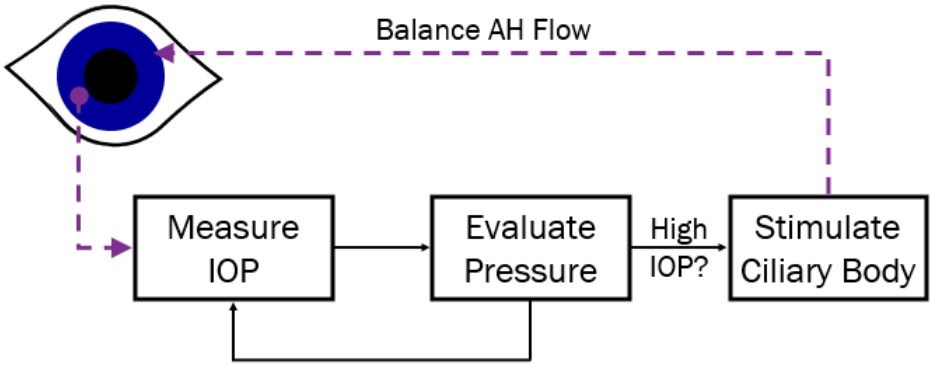

Figure 19: Closed Loop Block Diagram of the Ideal Device interacting with the intraocular environment.

To test this closed loop system, I modified the DataView software (using Python 3.6.1) and the breakout board version of the Bionode (both created by members of the CID) for the new application [38]. This system allowed me to wirelessly communicate between the pressure sensor circuitry, the stimulation circuitry, and a computer through the use of the DataView GUI. I modified the software to calibrate the input voltage from the Wheatstone bridge AFE to its corresponding pressure. I also created the code to have DataView initiate stimulation when the pressure reached certain thresholds. The parameters controlling this functionality can be manipulated by user inputs within the GUI (see Figure 20).

Benchtop testing was performed by connecting the Volcano sensor and Wheatstone bridge AFE to the Bionode breakout board. This testing was done to check that the environmental pressure was correctly displayed on DataView and that when the recorded pressure reached the threshold values, the stimulation was activated or deactivated.

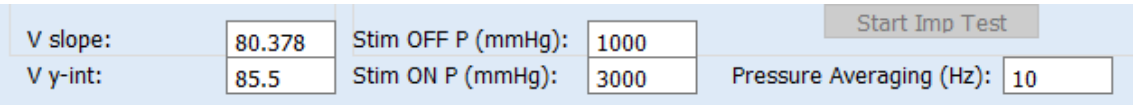

Figure 20: Editable Parameters added to Bionode DataView to allow the user to calibrate and control the closed loop implementation of the intraocular device.

I created a new daughter board (PCB created using Altium 18.1.6 and milled using the LPKF ProtoMat S100) with the filtered Wheatstone bridge circuitry to translate the resistances of the Volcano sensor into a voltage to be fed into channel 1 of the microcontroller on the Bionode. This AFE uses the 1.8 V, 0.9 V and GND rails created by the Bionode breakout board to power the Wheatstone bridge and the INA333 instrumentation amplifier. This AFE uses a 100x gain and a V1 of 0.9 V. The board also includes potentiometers to tune the resistances of the Wheatstone bridge to match the resistances on the Volcano sensor being used. This set up with the AFE as a daughterboard for the Bionode allows the closed loop system to be in one package, powered by a Micro-USB cable, with three inputs for the volcano sensor and two outputs for stimulation. The stimulation system of the Bionode used a Howland current pump (LT6375) based stimulation circuit and can provide up to ±1.05 mA of current with variable stimulation periods and duty cycles as defined by DataView [38].

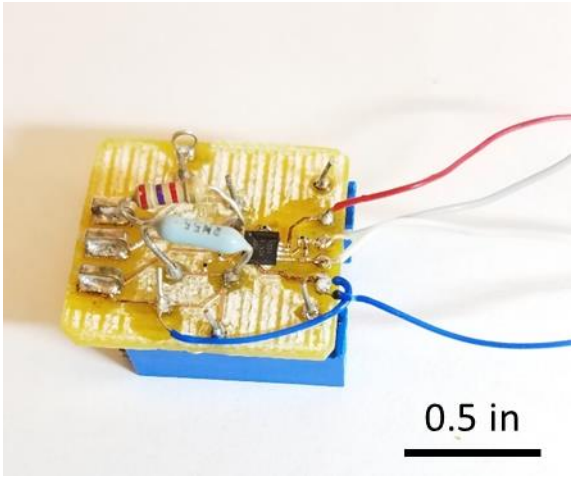

Figure 21: Wheatstone bridge daughter board for the Bionode breakout board. Includes voltage and resistance inputs and an output of the amplified voltage from the Wheatstone bridge. The potentiometers (blue components on underside of PCB) allow for calibration of the circuit to various Volcano sensors and their specific resistances.

Recordings using the Bionode are done by placing the Volcano sensor into a pressure chamber held at a constant pressure. The system samples the data at 6.25 or 12.5 kHz and averages the pressures to 10 Hz.

2.3 Device Form Factor, Packaging, and Insertion

The design of the intraocular ring involves not only the circuitry design to optimize the pressure sensing and stimulation circuitry, but also requires proper packaging to create the necessary form factor, stability and electrical functionality. The final device will consist of a gold on parylene (or similar) ring of coils, the Volcano piezoresistive sensor, and an ASIC (see Figure 22). These main components will be packaged into a flexible implant that can be inserted into the posterior chamber of the eye.

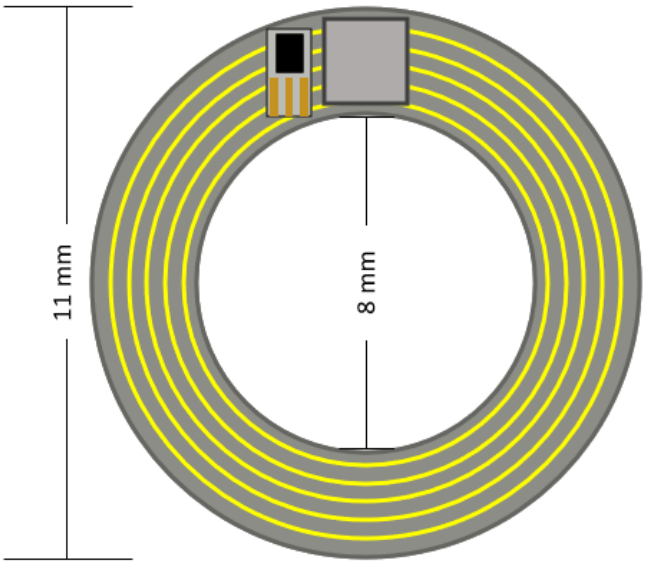

Figure 22: Mock-up for final Intraocular Ring Device. The components at the top of the image represent the Volcano Sensor and ASIC that will be attached to the electrical coils (gold colored rings).

The obvious constraint of the design is its size to fit into the posterior chamber, requiring a maximum outer diameter of 14 mm. In order for the device to be concealed behind the iris and not impede vision, the inner diameter of the packaged device should be greater than 8 mm [31]. The packaged device must also fold up to fit through a 4 mm slit for insertion through the cornea. The device also must have sufficient stability to protect the fragile components – notably the pressure sensor, ASIC, and wire-bonds. Inversely, the membrane of the sensor must remain exposed to the environment. The coils on the device must be properly connected. The stim coils must also be exposed to the environment while the powering and data transmission coils must be insulated to prevent shorting. The ring will likely have 5 coils. Two will be used for stimulation,

one for wireless powering, and two for wireless communication (both transmission and receiving).

2.3.1 Electrical Connections

The ASIC will be the main electrical component of the device. It must be electrically connected to the 3 pressure sensor terminals and the coils (data transmission, powering, and stimulation). The device may also require electrical connections to matched resistors or tuning capacitors for the Wheatstone bridge design and wireless powering respectively. The current method of creating electrical connections is to use wire-bonding to connect to the ASIC and pressure sensor pads and silver epoxy is used to attach to the gold rings. These connections must be insulated to prevent shorting. Current insulation methods include super glue to add increased stability and keep components from breaking and PDMS or silicon epoxy to allow for flexibility.

2.3.2 Exposed Sensor

The Volcano sensor membrane must stay exposed to the outside environment when fully packaged so that it can respond to the pressure of the environment. This adds additional challenges both for stabilizing the sensor on the device – it is one of the most fragile components – and for preventing shorts as the pressure sensor must be electrically connected and these connections must be insulated. Gel super glue has been used successfully to cover the wire-bonds and the electrical connections on the volcano sensor. The super glue must be applied precisely so as not to spread onto the membrane portion.

2.3.3 Insertion Tools

In the development of the packaging of the intraocular ring, the insertion method is important. One consideration is the methods currently used to insert other ophthalmic devices such as intraocular lenses [39] and capsular tension rings [40]. Both devices insert flexible structures into the eye through a small inserter that is introduced to the eye through the small slit in the cornea. Many IOL inserters (see Figure 23) have a chamber for the IOL to be folded into and a plunger is used to push the lens through a tube (2 mm inner diameter) into the interior of the eye. The capsular tension rings have a similar insertion technique except the ring is an open loop so that it can be inserted as a long, thin string and connected once inside the eye (see Figure 24).

Figure 23: Intraocular Lens inserter used in phacoemulsification surgeries.

Figure 24: Ophthalmologic Capsular Tension Ring Inserter.

I considered the use of an open loop package as done with the capsular tension ring as it would allow for the greatest ease in developing a package that would fit through an inserter. However, this idea is impractical due to the need to connect the electrical rings once implanted. The IOL style plunger also provided its own challenges; many of the wires inside the silicone or PDMS ring prototypes I designed were destroyed when pushed through the inserter due to the high strains placed on the ring. Additional methods of inserting were tested to reduce the strain on the wire. These methods include the use of different gauges of wire, different packaging materials, and methods of enclosing wire loops within the package.

2.3.4 Implantable Volcano Sensor

To create a testing device for the volcano senor, the sensor is attached to a small PCB (see Figure 25) with wires attached so the sensor can be attached to the Wheatstone bridge circuit.

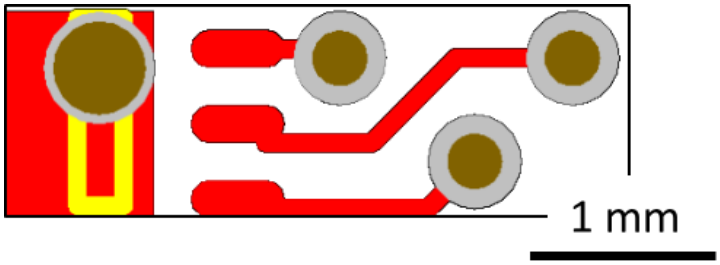

Figure 25: Altium schematic for the Volcano sensor PCB. The yellow rectangle is the designed location for the Volcano sensor. The circuit includes a via to keep the piezoresistive membrane open to the environment on both sides. The three pads on the Volcano Sensor are wire-bonded to the three traces and 36-gauge wires are soldered to the vias on those traces.

Once the board was milled, I use a scalpel to thin out the board in all dimensions. This is especially done to the thickness of the board by removing copper on the back side of the PCB and then continuing to remove a portion of the FR4 board from the backside. This leaves a thin layer of FR4 with the top side copper traces as the base for the volcano sensor. Next, I solder 36-gauge, stranded wire – used for size and flexibility – into the three vias. These wires are glued in place to increase stability and to ensure that all three wires came straight off the back side of the PCB, keeping the width of the board constant.

The sensor is then glued onto the PCB with care to keep the sensor portion exposed over the hole on the board and to make it flush to the board to avoid any cracking due to the applied pressure during the wire-boding stage. The wire-bonds are created between the Volcano sensor and the traces on the PCB. Once the board was fully electrically connected, the electrical connections are covered with super glue for insulation and stability. An additional layer of super glue is added to the distal end of the PCB so that the pressure sensor will not be pushed directly into the edge of the cornea during insertion.

2.3.5 Implantable Stimulation Ring

The intraocular stimulation rings were designed using clean room fabrication techniques by members of the CID. These are made of a parylene substrate with two gold rings (7 and 9 mm diameters) electroplated on top. After fabrication of the rings a 36-gauge stranded wire was attached to each ring using silver epoxy (MG Chemicals, #8331-14G) and super glue. The silver epoxy electrically connects the wire to the ring so that the stimulation coil can be attached to the circuitry creating the pulses.

2.4 Rabbit Surgery

In vivo testing of the prototypes is done by implanting the prototypes into the eye of New Zealand White rabbits. The rabbits are induced with a Ketamine/Xylazine mixture and are maintained under Isoflurane. Butorphanol is also injected for pain management. It was noted that proparacaine drops have an impact on IOP, therefore their use was eliminated from the procedures [8].

These tests are used for two main purposes – to better understand how the prototype devices will interact with the anatomy of the eye during and after insertion and to record IOP while stimulating the eye. The stimulation testing is to understand how different stimulation patterns influence IOP.

2.4.1 Phacoemulsification

The technique of phacoemulsification, described in more detail in the introduction, is used in our testing to imitate the surgery that would take place during the insertion of this ring into a human patient as this surgery would often piggyback on a cataract surgery. This technique also provides additional space in the posterior chamber for the placement of prototypes. Phacoemulsification begins with making a small (2.5-4.0 mm) slit into the cornea with a surgical knife. Through this, tools and materials can be passed into the anterior chamber. Methylcellulose (2% solution of Kitchen Alchemy, Methocel E4M) is injected into the eye to keep the eye inflated and transparent. Once the crystalline lens is removed (aspirated with a vacuum pump and saline irrigation), the prototype devices are inserted into the posterior chamber in the same way an IOL is placed in clinical applications.

2.4.2 Cannulation for Pressure Monitoring

An invasive blood pressure monitor (SurgiVet), connected to a cannula inserted into the eye, is used as a reference for monitoring IOP during surgical procedures. I create cannulas using 30G needles, non-silicone tubing, and a lure-lock connector on the proximal end so that it can be connected to the reference pressure sensor (see Figure 26). All connections on the cannulas are water proofed using super glue.

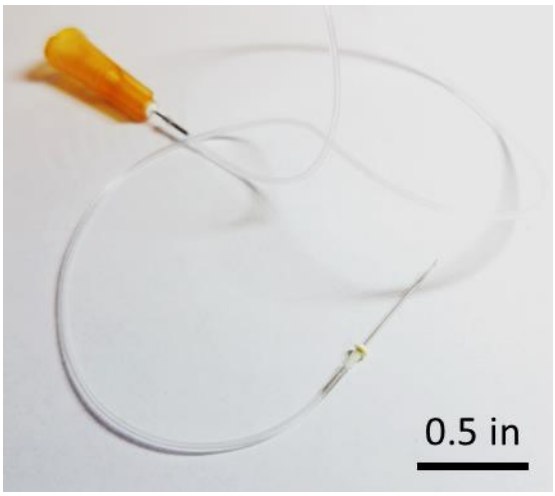

Figure 26: Cannula for monitoring IOP using the invasive blood pressure monitors. The orange colored lure lock connector attaches the cannula to the pressure sensor. The needle on the other end is inserted into the eye.

When inserting the cannula into the eye, the surgeon inserts the tip of the needle into the cornea without puncturing all the way through into the anterior chamber. The needle is then passed between the layers of the cornea and then, once a sufficient distance away from the initial entry point, the needle tip is used to puncture the interior layer of the cornea and enter the anterior chamber. This method creates a seal around the needle to prevent leakage. During the cannulation procedure, a back-pressure of approximately 25 mmHg is applied to the cannula and SurgiVet sensor (see Figure 27). This ensures that no fluid flows up the cannula and clogs the system as this scenario will lead to inaccurate results [41]. The output of the SurgiVet sensor is amplified using the INA333 and the voltage output is recorded using the NI DAQ controlled by a MATLAB script.

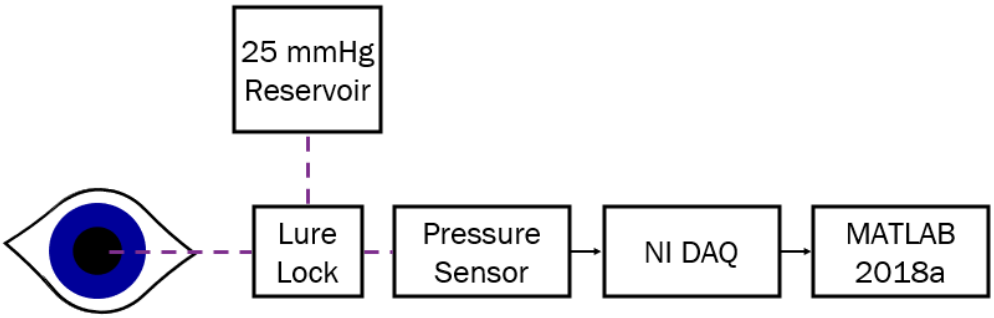

Figure 27: Block diagram of reference sensor cannula system (dashed lines representing pressure lines and solid lines representing electrical connections). The lure lock connection allows the reservoir to be connected to the system while cannulating the eye to provide a bias to the system and removed once cannulation is performed.

2.4.3 Intraocular Stimulation and Pressure Recording

Once the stimulation ring and Volcano sensor prototypes are inserted into the eye, I initiated the stimulation of the eye and monitored IOP using either the Volcano sensor or the cannulation set-up. The wires of the stimulation ring and Volcano sensor are attached to the Bionode breakout board and DataView is used to set the parameters and monitor pressure. The biphasic stimulation is defined by three parameters: pulse amplitude (μA), pulse width (μs), and pulse period (μs). Pulse period is the time between each stimulation pulse (positive or negative). Stimulation frequency (f in Hz) is related to the pulse period (PP as measured in μs) by equation (9).

$$f = \frac{10^6}{2PP} \tag{9}$$

The stimulation parameters are chosen for each trial based on those seen in previous literature and in the clinical trial (discussed in section 1.3). For these exploratory stimulation experiments, parameters were adapted during experiments to attempt to see repeated effects. Stimulation is typically applied for about 15 minutes with a rest time of approximately 5 minutes between trials.

To ensure that the pressure sensor is actually monitoring pressure in the environment of the eye, periodic "poke tests" are applied to the eye. These tests consist of gently probing the eye with a thin, blunt object (such as forceps) and noting if there is a corresponding increase in the pressure recording (typically 5-10 mmHg). A failure of this test indicates a lack of accurate pressure recording often due to the cannula becoming clogged.

2.4.4 Statistical Analysis of IOP response to Intraocular Stimulation

The recorded IOP is analyzed for statistical significance using Minitab 2018 statistical software. Recorded IOP data is averaged to 0.1 Hz and divided into stimulation and rest segments based on the stimulation activity occurring at the time of recording. IOP changes due to "poke tests," other noted manipulations of the eye, and perceived inaccurate sensor recordings due to high noise are discarded. The data segments immediately before, during, and immediately after a stimulation period are analyzed for difference in means (One-Way ANOVA test) and difference in data trends (Fit Regression model) during the three periods. Data is analyzed with a 95% confidence interval. This analysis results in a p-value representing significance of the change in mean IOP,

and two p-values representing the significance of the changes in trend (p-value slope 1 compares the stimulation data to the pre-stimulation data while p-value slope 2 compares pre-stimulation to post-stimulation data). This analysis also provides an average mean and slope for each time period. The directions of the mean and slope changes along with their statistical significances are compared to decide whether the stimulation caused a significant change in IOP. The mean and slope trends should follow the same patterns and should show a response during the stimulation period. The change in IOP during these significant stimulation periods is recorded as the difference between the pressure at the beginning of stimulation time and the peak (minimum or maximum) pressure over the stimulation time.

3. RESULTS

3.1 Pressure Sensing Circuitry Design

The final circuitry chosen for IOP monitoring with the Volcano Sensor is a low-pass filtered Wheatstone Bridge design with an instrumentation amplifier. The output of this discrete circuit has an unaveraged error of 0.289 mmHg (V1 = 1 V, Gain = 100x) over 5 minutes as shown in Table 3. This is a large improvement over many of the other designs (see Table 2). The Wheatstone bridge AFE provides the lowest measurement error of all the circuits tested with the exception of the LCR meter. It is also noted, based on my testing summarized in Table 2, that there is a significant decrease in the error resulting from a circuit designed on an ASIC as compared to the discrete design (see AFE 1 vs discrete AFE 1). This is an advantage as the final design chosen is a discrete circuit with a low measurement error which can be expected to decrease further as an ASIC.

Table 2: Measurement error of pressure measurement circuitry (unaveraged data) when tested with fixed resistors. The error is a measure of the standard deviation, evaluated over each 8-minute time period in the recordings. (Discrete AFE 1 was only recorded for 6.55 minutes)

Device	Measurement Error (mmHg) (Average ± Standard Deviation)	N
LCR Meter	0.76 ± 0.25	103
Hansraj ASIC	4.24 ± 0.73	426
AFE 1	4.33 ± 1.69	24
AFE 1 (2x Power)	4.07 ± 2.32	11
AFE 1 (4x Power)	3.04 ± 0.59	43
AFE 2	2.27 ± 0.48	54
Discrete AFE 1	12.18 ± N/A	1
Discrete AFE 1 Voltage References	10.34 ± 1.37	53
Discrete AFE 1 (2.5x Power)	6.18 ± 1.07	7
R-V AFE	14.05 ± 1.52	10
R-V AFE, Filtered	9.54 ± 0.54	4
Wheatstone Bridge	1.82 ± 0.23	3

The size of this circuit is currently about 1 in x 1 in, making it far larger than the specification, but will be modified into an ASIC that should be no larger than 1 mm x 1 mm including the stimulation, powering, and communication circuitry as well as the pressure monitoring.

Once I had developed the filtered Wheatstone Bridge circuit design, I evaluated how the various parameters such as gain and the input voltage (V1) for the Wheatstone bridge would affect the error at the output using the NI DAQ (see Table 3).

Understanding how these parameters affect the error, allows the final design to be optimized based on a number of factors. The higher the input voltage, the greater the power consumption of the device, therefore the design will ideally be optimized for a low V1. The gain will influence how well matched the resistors in the device will need to be to produce outputs within the range of the instrumentation amplifier (INA). A device with a higher gain will fill a larger fraction of the output range of the INA given the same input range. The closer the two voltage inputs of the INA are to each other – primarily affected by the resistances of the fixed resistors, the closer the output of the INA is to its reference. Therefore, devices with lower gains can tolerate a wider range of fixed resistances before causing a railed output of the INA.

Table 3: Low Pass Filtered Wheatstone Bridge pressure sensing circuit output error (unaveraged). Environment pressure was held constant at 0 mmHg. The pressure was recorded over 5 minutes at 1000 Hz with the NI DAQ.

Average Measurement Error (mmHg)					
	Input Voltage (V)				
Gain	**0.2**	**0.5**	**1**	**1.5**	**1.8**
1000x	0.225	0.178	0.170	0.123	0.107
100x	1.479	0.593	0.289	0.240	0.214
10x	9.199	3.799	1.873	1.847	1.363

This information shows that without averaging, the discrete system has errors below 0.5 mmHg for many of the V1, gain combinations. For the final device I chose a V1 as 0.9 V and a gain of 100x. This was chosen as 0.9 V is available on the breakout board I am designing for as my test device and the 100x gain is a lower gain that allows for the error to stay below 0.5 mmHg. To improve the accuracy of the device, this gain or the V1 voltage can be increased.

The final system, tested with the Volcano sensor in air at 0 mmHg, (recorded at 12.5 kHz and averaged to 10 Hz) had an 8-minute standard deviation of 0.53 ± 0.20 mmHg (N = 6). The error was also monitored at 15 mmHg resulting in an average error of 0.71 ± 0.59 mmHg (N =6). Figure 28 and Figure S4 show the recorded data over time and the measurement error over time, respectively. The increase error of this recording with respect to Table 3 is likely due, in part, to the resolution of the ADC (analog to digital converter) used on the Bionode breakout board (1.8 V/ 8-bits = 7 mV). Another likely factor is variability of the environmental pressure within the chamber – especially at the higher pressure.

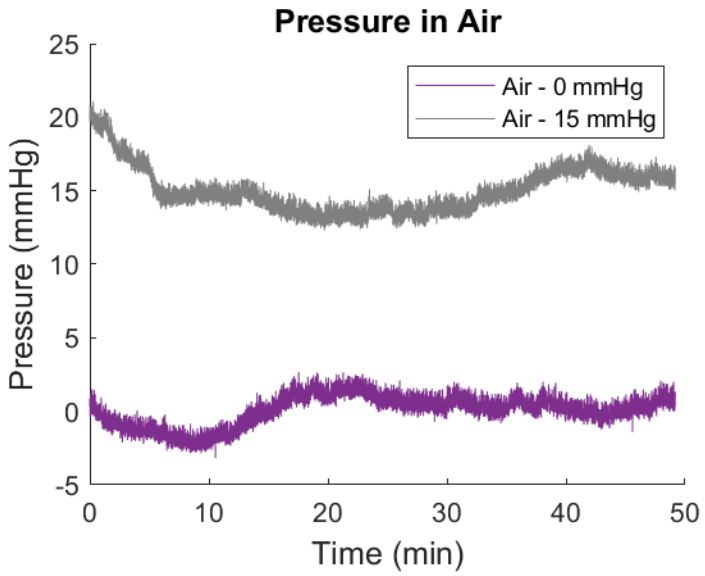

Figure 28: Recorded pressure over time (V1 = 0.9 V, Gain = 100x) at 0 and 15 mmHg respectively. Pressure was recorded at 1000 Hz and averaged to 10 Hz.

This AFE circuit draws approximately 295 µW of power for operation. The power is consumed in the form of 250 µA drawn from the 0.9 V sources and 38 µA drawn from the 1.8 V sources.

3.2 Miniaturized Discrete Intraocular Ring

To fully test the discrete intraocular ring, the input and output components must be miniaturized to fit within an eye. I created a system that included an implantable pressure sensor and an implantable stimulation ring as the interfacing input and output components. Both devices have thin wires (stranded 36-gauge) that will run through the slit in the cornea to the outside of the eye so that they can attach to the discrete circuitry.

The pressure sensor board (see Figure 29) final dimensions are 1.25 mm x 3 mm x 0.4 mm. This board is fully waterproofed and stabilized using a coating of super glue. The board's small width and thickness allows its insertion through the slit created in the cornea for phacoemulsification.

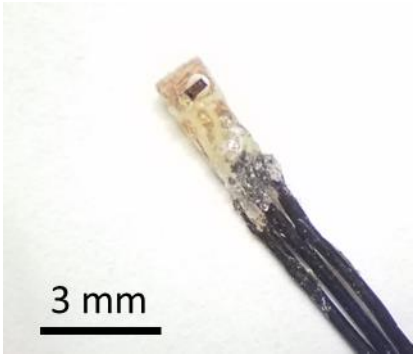

Figure 29: Implantable device for pressure sensing with the Volcano sensor (located at the top of the PCB). The wires at the end are threaded out of the cornea to connect to the circuitry.

The implantable stim ring (see Figure 30) is a gold on parylene design that was fabricated by other members of the CID in the clean room. The external wires are attached using silver epoxy with a coating of super glue for additional stability. This gold rings in the device have diameters of 9 mm and 7 mm. The paper-thin ring can be rolled and inserted with the use of an IOL inserter (see Figure 31).

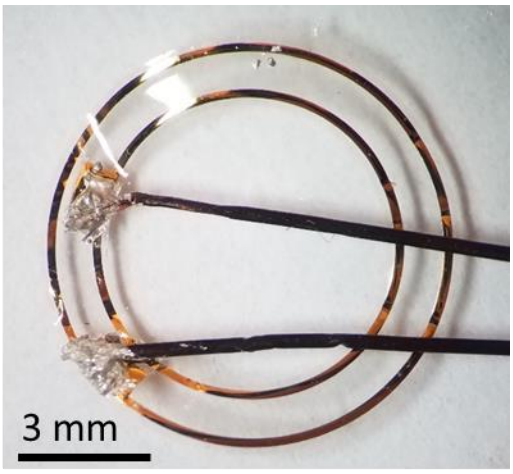

Figure 30: Implantable Stimulation Ring made of gold on parylene. The wires electrically connect the coils inside the eye to the circuitry outside the eye.

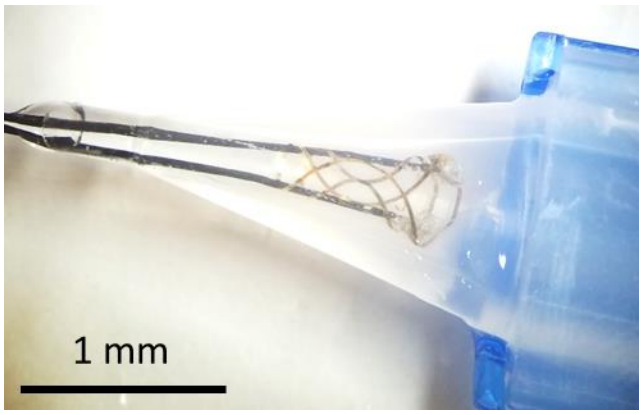

Figure 31: Stimulation ring inserted through an intraocular inserter.

The 36-gauge wires on both devices can be attached to the inputs of the daughterboard and the outputs of the stimulation board (Figure 32) respectively to create a complete the closed loop device.

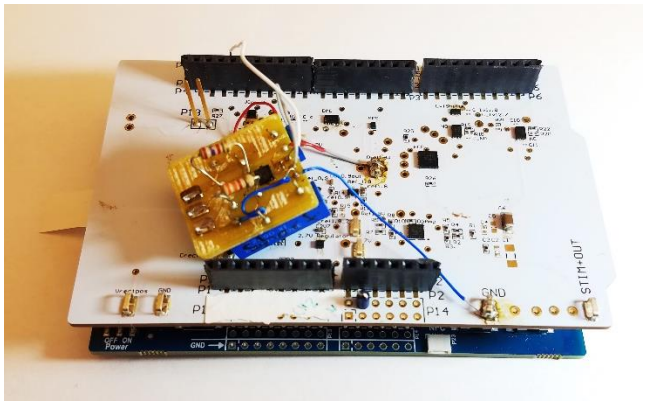

Figure 32: Bionode breakout board with added Wheatstone bridge daughter board.

The final version of the DataView software for the closed loop intraocular ring is shown in Figure 33. This software is used to display and calibrate the pressure readings and to turn on the stimulation as needed. The V slope and V y-int numbers are used to provide calibration from the input voltage of channel 1 to the pressure as shown in equation (10). The Stim OFF and Stim ON parameters are used to define the closed loop implementation of the program. They define where the stimulation is always off (P < Stim OFF), where the stimulation is always on (P > Stim ON). The range of pressures between Stim OFF and Stim ON will continue to either stimulate or not stimulate based on its previous state and can be manually toggled. The Pressure Averaging input is used to determine how much averaging is applied to the pressure output. This software

communicates with the device through the base station and the Bionode breakout board and completes the closed loop circuit of the implantable device.

$$P = V_{IN}V_{SLOPE} + V_{Y-INT} \quad (10)$$

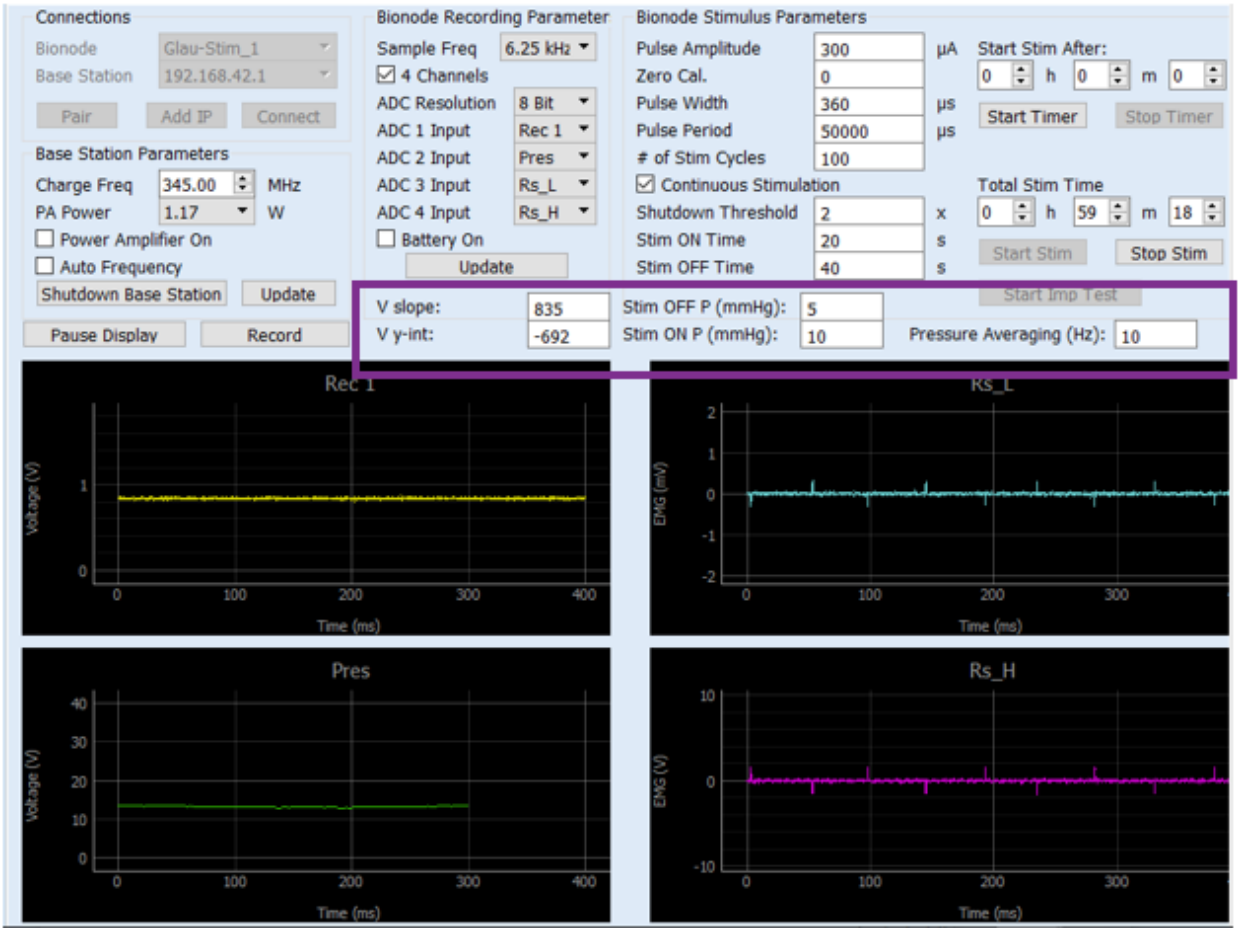

Figure 33: Bionode DataView GUI to display and calibrate both the pressure sensor input and the stimulation output. The GUI also controls the closed loop stimulation parameters. The boxed area shows the new features added to the GUI. Pressure in environment during recording was 14 mmHg.

3.3 In Vivo Trials

3.3.1 Intraocular Pressure Monitoring

Prior to implanting the device in a live rabbit, the implantable sensor was tested using a pig eye. In this test, I successfully simulated the intended experimental procedure by cannulating the pig eye and creating the small corneal incision through which the implantable sensor could be inserted (Figure 34). This test shows that the packaging is sufficient to protect the volcano sensor

and electrically connect it to an outside measurement circuit. The pressure was recorded using the implanted Volcano Sensor.

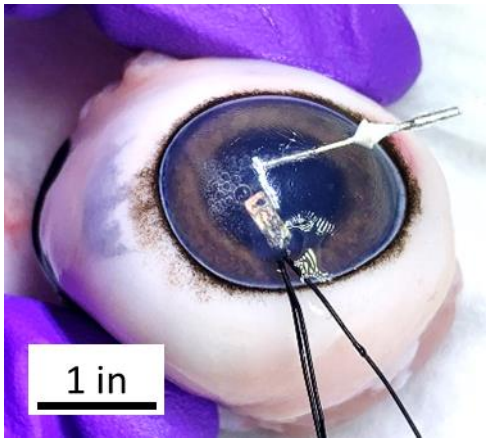

Figure 34: Implantable pressure sensor inserted into a cannulated porcine eye.

The calibrated pressure recorded from the pig eye is shown in Figure 35(a). The spikes in the time from about minute 2 to minute 3 occur because during this time we were adjusting the eye. These spikes show the sensor is responding to the pressure changes in the environment. A subset of the pressure recording is shown in Figure 35(b) to display the recorded pressure without the large pressure spikes.

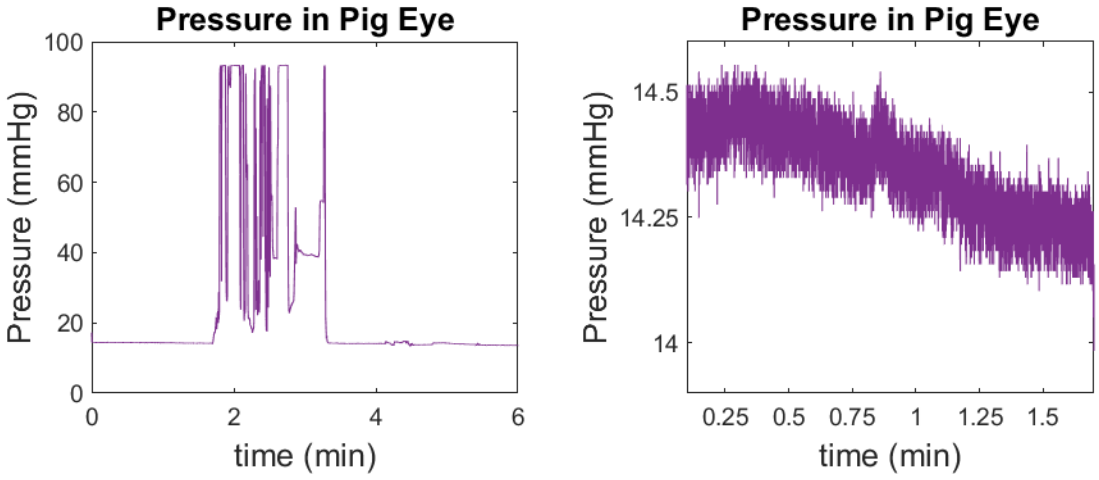

(a) (b)

Figure 35: Pressure recorded from Volcano sensor while in a porcine eye (a) and (b) a subset of that data. The spikes in (a) are accounted for are accounted for as actual events.

This pressure sensor was then implanted into a live rabbit eye for pressure data monitoring. This inserted device is shown in Figure 36. Super glue and sutures were used to close the corneal incision to prevent any leakage. The Volcano sensor was attached to the Wheatstone bridge AFE and breakout board to record pressure and create a closed loop with the implanted stimulation coil. This system was used to record the in vivo, rabbit IOP over time. An example of the in vivo Volcano pressure sensor recording is shown in Figure 37.

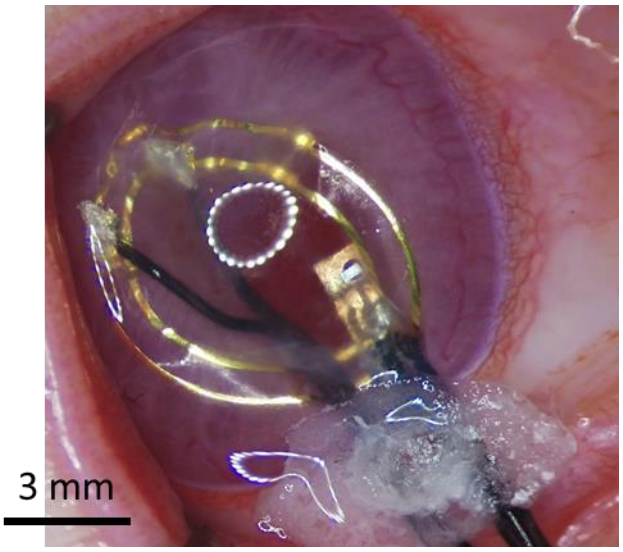

Figure 36: Implanted stimulation coil and Volcano sensor in a rabbit eye.

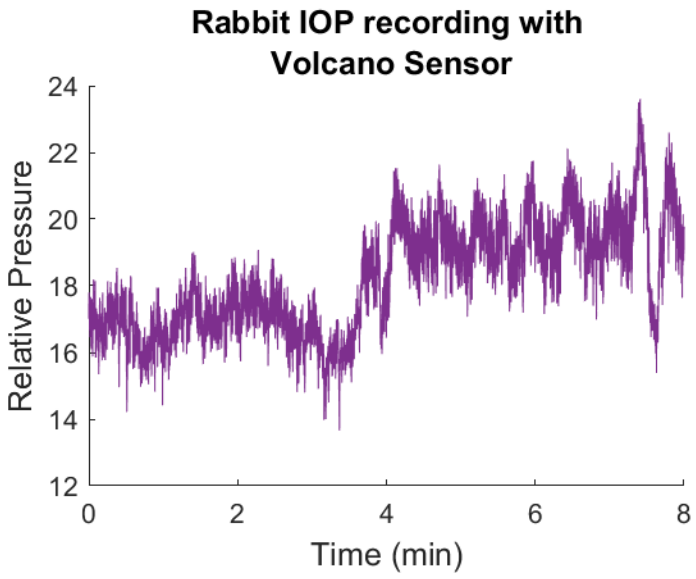

Figure 37: In vivo pressure recording using Volcano sensor in a rabbit eye.

3.3.2 Intraocular Stimulation

Intraocular stimulation was performed using the gold on parylene coil inserted into a live rabbit eye (see Figure 36). Stimulation was performed using the Bionode breakout board using a variety of stimulation parameters (summarized in Table S2).

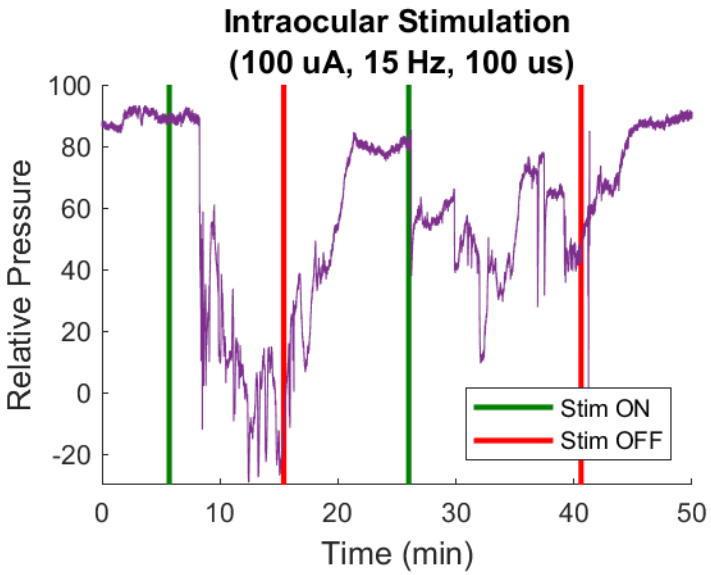

Figure 38: Example of IOP response to in vivo intraocular stimulation at 100 µA, 15 Hz, 100 µs. Green vertical lines represent the beginning of a stimulation period and red lines represent the end of the stimulation period. Stimulation performed in a rabbit eye.

Stimulation performed using this system caused repeated drops in IOP when stimulated using a 100 µA amplitude, 10-15 Hz stimulation frequencies, and 100-1000 µs pulse widths (an example shown in Figure 38). There may have been additional IOP changes at amplitudes between 50 µA and 300 µA (summarized in Figure 39).

Statistical Analysis was performed using One-Way ANOVA tests to compare the means of the IOP and Fit Regression models to compare the data trends. All tests were performed to compare the IOP data immediately preceding, during, and immediately after a stimulation period. The stimulation periods that had statistically significant and clinically significant (means and slopes increased or decreased together and changed with the stimulation) are shown in Table 4 (all results in Table S2) along with the change in the average IOP during and before stimulation.

Table 4: Significant IOP change responses to intraocular stimulation seen in an in vivo New Zealand White rabbit model.

Rabbit ID	Amplitude (μA)	Pulse Width (μs)	Frequency (Hz)	Mean IOP Change (mmHg)
NZR008	50	100	15	-5.16
NZR010	50	100	15	7.325
NZR012	75	2500	15	4.094
NZR010	100	100	10	-6.208
NZR008	100	100	15	-100.74
NZR008	100	100	15	-44.737
NZR008	100	100	15	-7.0235
NZR012	100	1000	15	-4.252
NZR012	100	1000	15	-2.6614
NZR008	200	100	15	0.515
NZR010	200	100	20	7.047
NZR008	300	100	15	0.371
NZR012	300	2500	15	1.229

These significant stimulations were used to form the stimulation response curve in Figure 39. The exceptionally large pressure drops (rows 5 and 6 of Table 4) in the first rabbit were not included in the stimulation response curve as they were likely subject to incorrect pressure calibration. The low sample size and the biological differences between animals may account for the large error bars shown in the stimulation response curve.

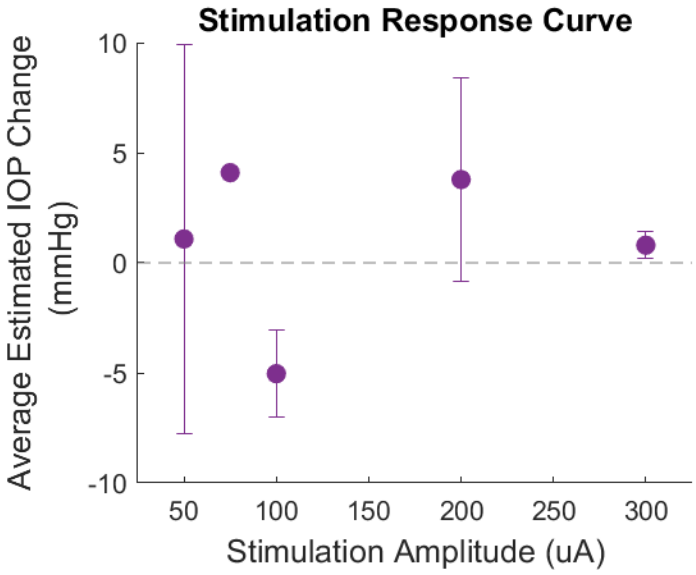

Figure 39: Stimulation response curve for in vivo pressure changes due to stimulation frequencies of 10-20 Hz (N = 2, 1, 4, 2, 2 respectively for stimulation amplitudes of 50 µA to 300 µA).

3.3.3 Closed Loop

The implantable versions of the Volcano Sensor and the Stimulation Ring were implanted in vivo into Rabbit eyes through a corneal incision (see Figure 36). These components were connected to the closed loop circuitry to monitor the intraocular pressure while stimulating the eye. During this experiment the DataView limits for starting or stopping intraocular stimulation were set outside the range of expected pressures to allow the stimulation parameters to be set manually to perform the stimulation experiments as outlined above. However, the closed loop system allowed for recording of stimulation and pressure data on the same device. This set up would allow for closed loop pressure recording and intraocular stimulation in future experiments as it was successfully used in closed loop under benchtop conditions.

3.3.4 Form Factor Insertions

The final device will be in the form of a flexible ring implanted into the posterior chamber of the eye. We inserted these prototype devices with the use of the IOL injectors. Rings made of parylene and gold and were inserted with intact electrical conductivity (see Figure 40(a)). In addition, rings made of PDMS and silicone mimic the size and shape of the expected final device (see Figure 40(b)). These rings both were successfully implanted individually into live rabbit eyes.

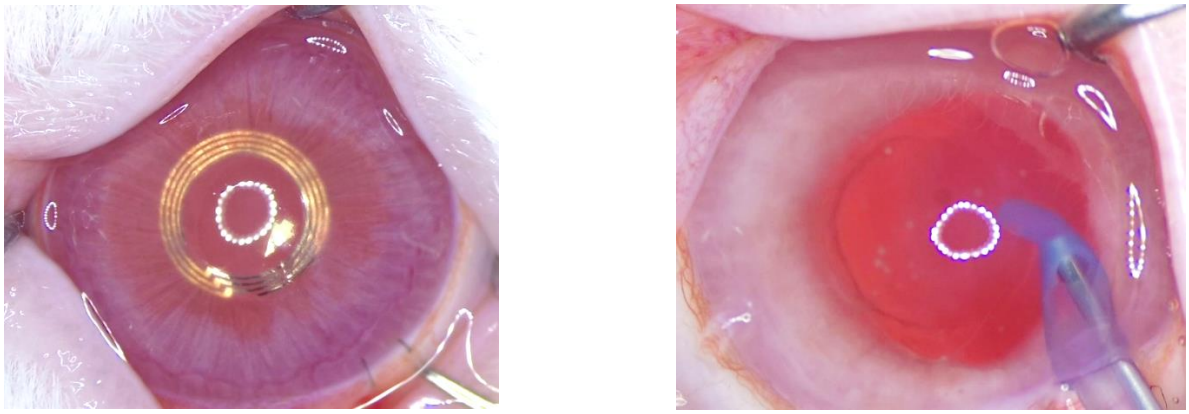

(a) (b)

Figure 40: Intraocular Rings implanted in vivo into rabbit eyes. (a) Gold on Parylene stimulation ring. (b) PDMS ring implanted into posterior chamber (the inner edge of the ring is visible in the red pupil just beyond the edge of the iris).

To successfully combine the electrically conductive rings with the size and shape of the expected device, a sandwich type ring was designed with two 50-gauge wire rings placed inside two thin silicone rings (see Figure 41). This designed allowed the wires to be enclosed within silicone without being stretched extensively during insertion. Parylene rings layered on a thin layer of silicone epoxy (thickness of approximately 0.3 mm) also were injectable using the IOL inserter without compromising the conductivity of the gold wire traces. The location of the parylene ring on the top of the silicone also allows the traces to be exposed for use as a stimulation ring.

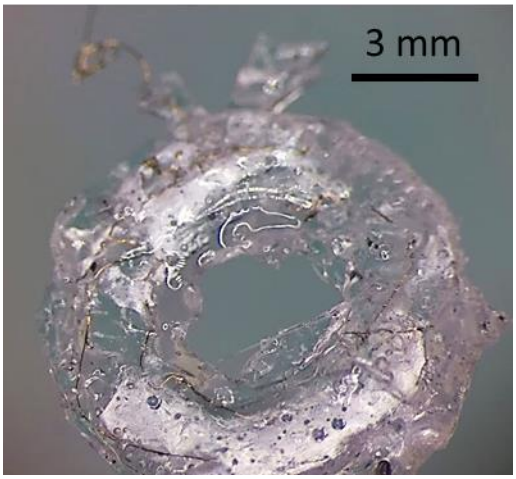

Figure 41: “Sandwich Ring” – made of silicone epoxy and 50-gauge wire. Wires are encased within, but not completely fixed to the silicone exterior.

The implantable stimulation ring and implantable Volcano sensor were also inserted into the anterior chamber of the rabbit eye through a corneal incision. Both devices were implanted through an incision of 2.85 mm. These devices were able to maintain functionality in vivo after being inserted.

4. DISCUSSION

4.1 Intraocular Ring Design Goal Overview

The aim of this project is to create a discrete version of a closed loop intraocular device for the treatment of glaucoma. This device provides therapeutic stimulation to the structures of the eye based on the current ocular pressure. The discrete device is used to define the parameters and circuitry that will be incorporated into the final ASIC design.

Pressure sensing, done by the Volcano Sensor, inputs into the closed loop circuitry. A Wheatstone bridge – one side being the Volcano sensor and the other is fixed resistors that are well matched to the resistances of the Volcano Sensor – whose output voltages are low-pass filtered and amplified is the ideal pressure sensing circuitry. The resultant pressure is evaluated by parameters (to be determined through further clinical evaluations) to activate the stimulation circuitry. The stimulation circuitry used in the discrete device is a Howland current pump that in its current configuration can output up to 1.05 mA of current [38]. This circuitry then outputs the necessary stimulation pulses – 100 µA, 100 µs, 15 Hz, biphasic stimulation based on current evaluations – to lower the IOP. It is hypothesized that the stimulation is acting on the ciliary body of the eye to influence a change in the flow of aqueous humor. This change in flow acts to reduce IOP and to thereby reduce the debilitating effects of glaucoma

4.2 Design Metrics

The design metrics for sensing accuracy, size, stimulation current, biocompatibility, and power consumption are outlined in Table 1. The final device has a pressure sensing accuracy of 0.53 mmHg. The power draw of the AFE portion is 295 µW. This is less than 6% of the desired specification as a discrete device, therefore, it is expected that the entire device will meet specification.

The sizes of the current components are 1.25 mm x 3 mm x 0.4 mm for the implantable pressure sensor and 9 mm outer diameter (OD), 7 mm inner diameter (ID) for stimulation ring plus the added 36-gauge wires. Given these dimensions, it is estimated that the combined, wireless device will have an OD of 10 mm, an ID of 7 mm, and a thickness of 1 mm. This does not meet the

inner diameter specification, however as the major component controlling this dimension is the parylene ring, this design could be modified to increase the ID. This design will fit within an incision of ≤ 4 mm.

4.3 Comparison to other Pressure Sensing Systems

This work is compared to other designs in Table 5. The additional sensing systems compared are Hansraj's ASIC [35], the SurgiVet invasive blood pressure monitoring system [36], and the Eyemate system [21]. The Eyemate device's error is based on that reported in [21], while the others are based on in house testing as summarized above. The SurgiVet system is listed as a comparison, although it is not implantable.

Table 5: Comparison of pressure sensor metrics.

	This Work	**Hansraj ASIC**	**SurgiVet**	**Eyemate**
Random Error	0.53 mmHg	6.8 mmHg	2 mmHg	0.81 mmHg
Device Size (mm)	10 x 10 x 1	3 x 3 x 0.5	LARGE	11.3 x 11.3 x 0.9
Inner Diameter	7 mm	> 8 mm	0 mm	7 mm
Incision Size	< 4 mm	< 3 mm	N/A	4 mm
Power Consumption	0.295 mW	0.0489 mW	35 mW	0.75 mW

The system I designed presents a highly competitive method of measuring IOP given its error, size and power consumption. This device also presents the unique feature of closed loop intraocular stimulation feedback to lower IOP.

4.4 Future Considerations

Continuation of this work will primarily consist of miniaturizing the device to an implantable package including both wireless powering and wireless data transmission. The miniaturization process into an ASIC will include creating the pressure sensing and stimulation circuits used in my design as CMOS (complementary metal-oxide semiconductor) layouts and designing the CMOS circuitry to translate the pressures to stimulation parameters, to output the data wirelessly, and to receive wireless power.

The miniaturization process will also include further refinement of the packaging techniques. As the device becomes smaller, additional precision can be gained by using a clean room such as parylene on oil [18] or photoresist sacrifice-replacement [42] techniques. These methods will insulate and secure the components without covering the membrane of the Volcano sensor.

Once this final packaging for the device is designed, it will need to undergo testing for mechanical reliability and longevity once it is implanted. This package will also require biocompatibility testing once completed.

In order to complete the design of the ASIC, additional surgical experiments will need to be completed to continue to define what stimulation parameters are needed based on various pressure readings.

4.5 Conclusions

Glaucoma research has shown a need for improved treatments for this irreversible disease. Research has shown the efficacy of electroceutical treatments in lowering IOP. Electroceutical treatments are ideal because of their ability to quickly lower IOP without causing major systemic effects. Medical treatments can also be improved by implementing them in a closed loop manner. The use of patient data to influence and update dosages, optimizes the results of treatment. A closed loop, electroceutical device for the treatment of glaucoma will stimulate the eye to induce a reduction in IOP with an intraocular, pressure-sensing, feedback loop. The main considerations for this device are pressure sensing accuracy, power consumption, and size.

To accurately monitor the piezoresistive Volcano sensor chosen for this application, I designed an analog front end circuit to convert the resistances of the sensor into a voltage, linearly related to the pressure in the environment. This AFE is based on a Wheatstone bridge design and also includes low pass filtering and signal amplification. This device has an error of 0.53 mmHg when recorded with an 8-bit ADC and consumes 295 µW of power. It does not currently meet the necessary size constraints and will need to be made into an ASIC to allow for ocular implantation. Other advantages of converting this circuit to an ASIC include the expected decrease of the noise floor and power consumption.

This data was then processed by Python software and a stimulation current was produced using a Howland current pump-based circuitry. This was done through the adaptation of the Bionode

breakout board and DataView software for use in the device. The output of the stimulation feeds into a two-ringed gold coil to output the electroceutical treatment. Stimulation through this setup showed decreases in IOP (in vivo New Zealand White rabbits) when performed with stimulation at 100 µA, 100 µs, and 15 Hz. This system is also far too large for ocular implantation and will need to be combined onto the AFE ASIC in future work.

In vivo testing of the device prototypes is performed using a New Zealand White rabbit model. As the circuitry of the device is not currently of an implantable size, the input and output devices alone can be inserted into the eye with connections to the external circuitry. Both the implantable Volcano sensor and the implantable stimulation ring able to be inserted through a corneal incision of 2.85 mm and have wires connected that run through the cornea to connect them to the closed loop circuitry.

A closed loop, electroceutical ophthalmic device will provide much needed, increased efficacy in the treatment of glaucoma. I have created a discrete version of this device using primarily off-the-shelf components that accurately measures and lowers IOP in vivo. Once this circuitry is adapted into an ASIC, the device will be a fully implantable, closed loop method of glaucoma treatment.

REFERENCES

[1] Y. Tham, X. Li, T. Y. Wong, H. A. Quigley, T. Aung, and C. Cheng, “Global prevalence of glaucoma and projections of glaucoma burden through 2040,” *Ophthalmology*, vol. 121, no. 11, Nov., pp. 2081–2090, 2014.

[2] H. A. Quigley and A. T. Broman, "The number of people with glaucoma worldwide in 2010 and 2020," *British Journal of Ophthalmology*, vol. 90, no. 3, Mar., pp. 262-267, 2006.

[3] National Eye Institute, “Glaucoma, Open-angle,” *National Institutes of Health*. [Online]. Available: https://nei.nih.gov/eyedata/glaucoma. [Accessed: 22-Mar-2019].

[4] National Eye Institute, “Facts About Glaucoma,” *National Institutes of Health*, Sept. 2015. [Online]. Available: https://nei.nih.gov/health/glaucoma/glaucoma_facts. [Accessed: 22-Mar-2019].

[5] Vision Eye Institute, “The vitreous humour,” *Vision Eye Institute*, Aug. 2017. [Online]. Available: https://visioneyeinstitute.com.au/eyematters/the-vitreous-humour/. [Accessed: 22-Mar-2019].

[6] L. Levin, S. Nilsson, J. V. Hoeve, S. Wu, P. Jaufman, and A. Alm, *Adler’s Physiology of the Eye*, 11th ed. Saunders, 2011.

[7] M. Wiederholt, H. Thieme, and F. Stumpff, “The regulation of trabecular meshwork and ciliary muscle contractility,” *Progress in Retinal and Eye Research*, vol. 19, no. 3, May, pp. 271–295, 2000.

[8] D. H. McDougal and P. D. Gamlin, “Autonomic control of the eye,” *Comprehensive Physiology*, vol. 5, no. 1, Jan., pp. 439-473, 2015.

[9] S. A. Bello, C. L. Passaglia, “A wireless pressure sensor for continuous monitoring of intraocular pressure in conscious animals,” *Annals of Biomedical Engineering*, vol. 45, no. 11, Nov., pp. 2592-2604, 2017.

[10] American Academy of Ophthalmology, “Intraocular pressure,” *American Academy of Ophthalmology*. [Online]. Available: https://www.aao.org/ [Accessed: 22-Mar-2019].

[11] “Aqueous Humour: Anatomy & Physiology,” *Medicalopedia*, Sept. 2012. [Online]. Available: https://www.medicalopedia.org/3183/aqueous-humour-anatomy-physiology. [Accessed: 22-Mar-2019].

[12] The Glaucoma Foundation, “Treating Glaucoma,” *The Glaucoma Foundation*. [Online]. Available: https://www.glaucomafoundation.org/treating_glaucoma.htm. [Accessed: 22-Mar-2019].

[13] The American Society of Health-System Pharmacists, “Timolol Ophthalmic,” *Medline Plus,* Apr. 2017. [Online]. Available: https://medlineplus.gov/druginfo/meds. [Accessed: 25-Mar-2019].

[14] G. Beidoe and S. Mousa, "Current primary open-angle glaucoma treatments and future directions," *Clinical Ophthalmology*, vol. 6, Oct., pp. 1699-1707, 2012.

[15] R. Suzuki, C. Dickens, A. Iwach, H. Hoskins, J. Hetherington, R. Juster, P. Wong, M. Klufas, C. Leong, and N. Nguyen, "Long-term follow-up of initially successful trabeculectomy with 5-fluorouracil injections," *Ophthalmology,* vol. 109, no. 10, Oct., pp. 1921-1924, 2002.

[16] “Pressure Sensor Drift,” Solinst, 2018. [Online]. Available: https://www.solinst.com. [Accessed: October 27, 2018].

[17] R. Otmani, N. Benmoussa, and B. Benyoucef, “The thermal drift characteristics of piezoresistive pressure sensor,” *Physics Procedia*, vol. 21, pp. 47-52, 2011.

[18] A. Agarwal, A. Shapero, D. Rodger, M. Humayun, Y. Tai, and A. Emami, “A wireless low drift implantable intraocular pressure sensor,” *IEEE Custom Integrated Circuits Conference,* Apr., 2018.

[19] “Verrata Pressure guide wire,” *Philips*. [Online]. Available: https://www.usa.philips.com/healthcare/medical-products. [Accessed: 22-Mar-2019].

[20] “The Solution: Eyemate,” *Implandata Ophthalmic Products*. [Online]. Available: https://implandata.com/EN/eyemate.html. [Accessed: 22-Mar-2019].

[21] A. Todani, I. Behlau, M. A. Fava, F. Cade, D. G. Cherfan, F. R. Zakka, F. A. Jakobiec, Y. Gao, C. H. Dohlman, and S. A. Melki, “Intraocular pressure measurement by radio wave telemetry,” *Investigative Ophthalmology and Visual Science,* vol. 20, no. 13, Dec., pp. 9573-9580, 2011.

[22] “Successful First-in-Human Testing of Implandata's Next Generation EYEMATE Micro-Sensor for Improved Monitoring of Glaucoma Patients,” *B3C newswire*, Nov. 17, 2017. [Online]. Available: https://www.b3cnewswire.com. [Accessed: 22-Mar-2019].

[23] S. Mishra, “Electroceuticals in medicine – the brave new future,” *Indian Heart Journal*, vol. 69, no. 2, Sept.-Oct., pp. 685-686, 2017.

[24] P. P. Irazoqui, G. Simon, G. Albors, J. Williams, Q. Yuan, Z. Wang, and C. Slaubaugh, “Multi-coil wireless power transfer assembly for wireless glaucoma therapy,” International Patent, 2019/028474A, 06 Aug., 2018.

[25] R. Nataloni, “IOP-Reducing 'Electroceutical' Eyeglasses Are Generating Buzz,” *MillennialEYE*, Nov.-Dec. 2017. [Online]. Available: https://millennialeye.com. [Accessed: 22-Mar-2019].

[26] R. Uusitalo, “Effect of sympathetic and parasympathetic stimulation on the secretion and outflow of aqueous humour in the rabbit eye,” *Acta Physiologica Scandinavica*, vol. 86, no. 3, Nov., pp. 315–326, 1972.

[27] C. Belmonte, S. P. Bartels, J. H. Liu, A. H. Neufeld, “Effects of stimulation of the ocular sympathetic nerves on IOP and aqueous humor flow,” *Investigative Ophthalmology and Visual Science*, vol. 28, no. 10, Oct., pp. 1649-1654, 1987.

[28] J. Gallar, J. H. Liu, “Stimulation of the cervical sympathetic nerves increases intraocular pressure,” *Investigative Ophthalmology and Visual Science*, vol. 34, no. 3, Mar., pp. 596-605, 1993.

[29] E. J. Linebarger, D. R. Hardten, G. K. Shah, R. L. and Lindstrom, “Phacoemulsification and Modern Cataract Surgery,” *Survey of Ophthalmology*, vol. 44, no. 2, Sept. – Oct., pp. 123-147, 1999.

[30] “CapsuleGuard I/A Handpiece Stellaris System 45°” *Storz Ophthalmic Instruments*. [Online]. Available: https://www.storzeye.com/products. [Accessed: 22-Mar-2019].

[31] R. H. Spector, “The Pupils,” in *Clinical Methods: The History, Physical, and Laboratory Examinations*, 3rd ed., H. K Walker, W. D. Hall, and J. W. Hurst, Eds. Boston: Butterworths, 1990.

[32] J. Nguyen and L. Werner, “Intraocular Lenses for Cataract Surgery,” in *Webvision: the organization of the retina and visual system*, H. Kolb, E. Fernandez, and R. Nelson, Eds. Bethesda, MD: National Library of Medicine (US), 2007.

[33] American Academy of Ophthalmology, “Normal Crystalline Lens,” *American Academy of Ophthalmology*. [Online]. Available: https://www.aao.org/. [Accessed: 22-Mar-2019].

[34] L. Luo, H. Lin, M. He, N. Congdon, Y. Yang, and Y. Lui, “Clinical evaluation of three incision size–dependent phacoemulsification systems,” *American Journal of Ophthalmology*, vol. 153, no. 5, May, pp. 831-839, 2012.

[35] H. Bhamra, J. Tsai, Y. Huang, Q. Yuan, J. V. Shah, and P. Irazoqui, “A subcubic millimeter wireless implantable intraocular pressure monitor microsystem,” *IEEE Transactions on Biomedical Circuits and Systems*, vol. 11, no. 6, Dec., pp. 1204–1215, 2017.

[36] “Invasive Pressure Accessories,” *Smiths Medical*. [Online]. Available: https://www.smiths-medical.com/products/veterinary/monitoring/monitoring-accessories/invasive-pressure-accessories. [Accessed: 22-Mar-2019].

[37] E. L. Spotts, D. P. Newman, and R. E. Farreau, “Pressure sensor,” U. S. Patent 5,042,495A, 27 Aug., 1991.

[38] D. J. Pederson, C. J. Quinkert, M. A. Arafat, J. P. Somann, J. D. Williams, R. A. Bercich, Z. Wang, G. O. Albors, J. G. Jefferys, and P. P. Irazoqui, “The bionode: a closed-loop neuromodulation implant,” *ACM Transactions on Embedded Computing Systems*, vol. 18, no. 1, Feb., pp. 1-20, 2019.

[39] “Loadinject,” *MDJ*. [Online]. Available: https://m-d-j.com/. [Accessed: 22-Mar-2019].

[40] R. Menapace, O. Findl, M. Georgopoulos, G. Rainer, C. Vass, and K. Schmetter, “The capsular tension ring: designs, applications, and techniques,” *Journal of Cataract and Refractive Surgery*, vol. 26, no. 6, Jun., pp. 898-912, 2000.

[41] M. Härkönen, A. Palkama, and R. Uusitalo, “Functional Dependence of the Ciliary Epithelium ATPase Activity and Intraocular Pressure on the Autonomic Nervous System,” *Acta Physiologica Scandinavica*, vol. 86, no. 3, Nov., pp. 327–341, 1972.

[42] L. T. Chen, J. S. Chang, C. Y. Hsu, and W. H. Cheng, “Fabrication and Performance of MEMS-Based Pressure Sensor Packages Using Patterned Ultra-Thick Photoresists,” *Sensors*, vol. 9, no. 8, Aug., pp. 6200–6218, 2009.

SUPPLEMENTARY INFORMATION

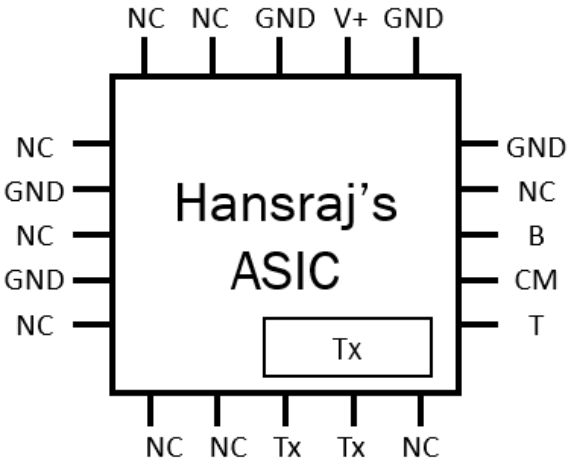

Figure S1: Hansraj ASIC IO Pad Schematic. V+ pads require an input voltage of 1.8 V. The pads B, CM, and T connect to the respective Volcano sensor pads. The Tx pads are connected to a 2.4 mm loop for the transmission of digital data. NC (no connect) pads are left open.

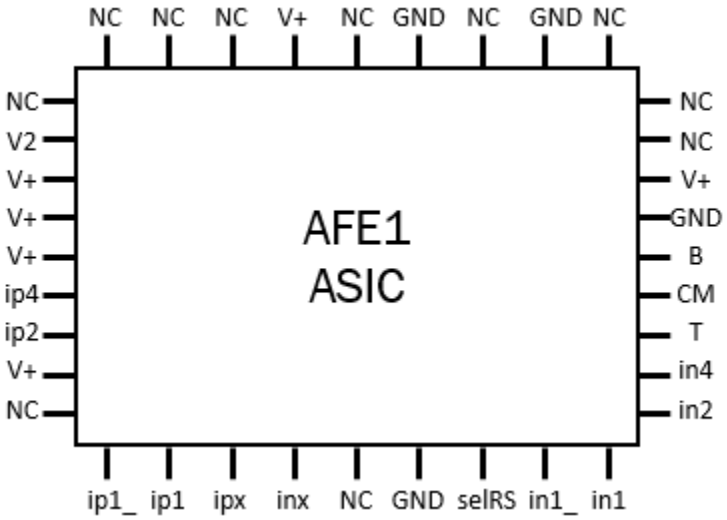

Figure S2: AFE 1 ASIC IO Pad Schematic. V+ pads require an input voltage of 1.35 V and V1 is supplied 1.8 V. The pads B, CM, and T connect to the respective Volcano sensor pads. The output pads are labeled as in1, ip1, in2, etc. and output a current. NC (no connect) pads are left open.

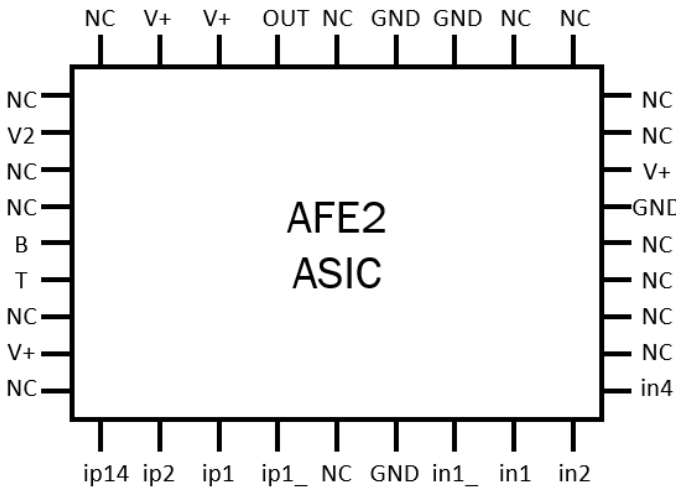

Figure S3: AFE 2 ASIC IO Pad Schematic. V+ pads require an input voltage of 1.35 V and V1 is supplied 1.8 V. The pads B and T connect to the respective Volcano sensor pads. The output pads are labeled as in1, ip1, in2, etc. and output a current. NC (no connect) pads are left open.

Table S1: ESD Protection Evaluation of Pressure Sensor

	Voltage across R_B (V)			**Voltage across R_T (V)**		
		Actual			**Actual**	
V_{DD} (V)	**Expected**	**T = High**	**B = High**	**Expected**	**T = High**	**B = High**
0.3	0.157	0.159	0.158	0.143	0.144	0.144
0.6	0.314	0.316	0.315	0.286	0.286	0.287
0.7	0.367	0.368	0.367	0.333	0.334	0.335
0.8	0.419	0.421	0.415	0.381	0.381	0.387
0.9	0.472	0.473	0.429	0.428	0.429	0.472
1	0.524	0.525	0.393	0.476	0.476	0.617
2	1.048	1.05	0.314	0.952	0.951	1.684

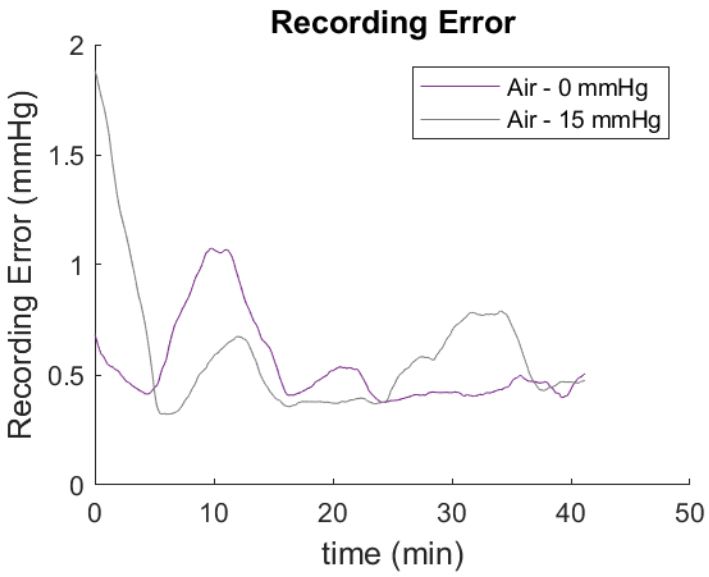

Figure S4: The 8-minute standard deviations of data (see Figure 28) recorded with the final AFE system on the Bionode breakout board. Recordings were done in air at 0 mmHg and 15 mmHg.

Table S2: Statistical Analysis of intraocular stimulation data from New Zealand White rabbit model. P-values shown represent the results of One-Way ANOVA (mean) and Fit Regression Model (slope 1 and 2) statistical analysis completed in Minitab on the pressure recorded during stimulation and compared to the IOP of the times immediately preceding and following it.

Rabbit ID	Amp (μA)	Freq (Hz)	p-value (Mean)	p-value (Slope1)	p-value (Slope2)	Significant Results	Comments
NZR008	100	50	0.000	0.003	0.000	NO	Opposite results
NZR008	400	50	0.000	0.171	0.000	NO	Opposite results
NZR008	500	50	0.000	0.094	0.399	NO	
NZR008	600	50	0.000	0.015	0.018	NO	Constant Decrease
NZR008	700	50	0.000	0.229	0.000	NO	
NZR008	100	50	0.000	0.404	0.000	NO	
NZR008	100	15	0.000	0.000	0.000	Decrease	
NZR008	100	15	0.000	0.000	0.000	Decrease	
NZR008	300	15	0.000	0.000	0.000	Increase	Local Increase
NZR008	200	15	0.005	0.000	0.002	Increase	Local Increase
NZR008	50	15	0.000	0.000	0.503	Decrease	
NZR008	100	15	0.000	0.001	0.006	Decrease	
NZR010	100	15	0.000	0.000	0.671	NO	High Noise
NZR010	50	15	0.000	0.000	0.965	Increase	
NZR010	200	15	0.000	0.278	0.249	NO	
NZR010	200	15	0.000	0.867	0.000	NO	Recording Error
NZR010	100	10	0.001	N/A	0.000	Decrease	No Pre-Data
NZR010	125	10	0.008	0.312	0.021	NO	Opposite results
NZR010	75	10	0.000	0.65	0.000	NO	Opposite results
NZR010	300	20	0.000	0.000	0.000	NO	Constant Decrease
NZR010	200	20	0.000	0.004	0.879	NO	Constant Decrease
NZR010	200	20	0.000	0.000	0.045	Increase	
NZR012	100	15	0.000	0.000	0.039	NO	Opposite results
NZR012	100	15	0.78	0.000	0.47	Decrease	
NZR012	100	15	0.000	0.000	0.000	Decrease	
NZR012	200	15	0.000	0.926	0.016	NO	External Factors
NZR012	300	15	0.000	0.000	0.261	NO	External Factors
NZR012	100	15	0.000	0.000	0.000	NO	External Factors
NZR012	100	15	0.009	0.000	0.000	NO	Constant Increase
NZR012	300	15	0.000	0.000	0.012	Increase	
NZR012	75	15	0.000	0.000	0.907	Increase	
NZR012	100	10	0.000	0.417	0.909	NO	